

Major and Trace Element Concentrations in Chromite and Silicate Minerals of the Critical Zone of the Bushveld Complex, South Africa: Effects of Reequilibration and Crystal Fractionation on Chromite Composition

Sarah-Jane Barnes,^{1,†} Wolfgang D. Maier,² Dany Savard,¹ and Stephen A. Prevec³

¹*Sciences de la Terre, Université du Québec à Chicoutimi, Québec G7H 2B1, Canada*

²*School of Earth and Environmental Sciences, Cardiff University, Wales CF10 3AT, UK*

³*Department of Geology, Rhodes University, Makhanda 6140, South Africa*

Abstract

The Rustenburg Layered Suite of the Bushveld Complex, South Africa, contains the world's largest resource of chrome and platinum group elements (PGEs). Both Cr and PGEs are found in chromitite layers within an approximately 1,000-m-thick section of ultramafic to mafic rocks known as the Critical zone. Neither the process of how the chromitite layers form nor the role that chromite plays in collecting the PGEs is clear.

Major and trace element contents of chromite and silicate minerals from each of the 13 chromitite layers, and from chromite in the adjacent peridotites and norites, have been determined. The concentrations of PGEs in both chromite and silicates are less than detection levels (10–20 ppb). Thus, neither are the host of the PGEs in these rocks.

The Cr# and Fe# of the chromites from chromitite layers are similar to those found in experiments carried out to model the crystallization of the initial magma (B1) of the Bushveld, with the same decrease in Cr# with increase in Fe#. The f_{O_2} of the experiments $\Delta 0$ FMQ (where FMQ = fayalite-magnetite-quartz buffer) and those of the chromitite chromite calculated from the Fe^{3+}/Fe_{Total} ratios and the V contents of the chromite are similar. Variations in trace element contents of the chromitite chromite can also be modeled using the B1 composition and allowing for ~40% crystal fractionation across the stratigraphy.

Introduction

Chromite is one of the first minerals to crystallize from mafic and ultramafic melts; thus, the composition of chromite in volcanic rocks could potentially indicate the composition of the primary melts (Barnes and Roeder, 2001; Kamenetsky et al., 2001). However, in volcanic rocks it has been shown that as the liquid fractionates, chromite composition reequilibrates with the more fractionated liquid (Scowen et al., 1991; Barnes, 2024). Furthermore, after solidification chromite exchanges elements with the silicate minerals or glass (Lenaz et al., 2012; Bai et al., 2021). Cooling in plutonic rocks is slower than in volcanic rocks, and hence the tendency for both super- and subsolidus reequilibration to occur is more likely. In addition, the degree of change in composition of chromite depends on the proportion of silicate minerals to chromite, with disseminated and matrix chromite tending to reequilibrate to a greater degree than chromite in chromitites (Roeder and Campbell, 1985; Teigler and Eales, 1993; Langa et al., 2021). Following the definition in the *Glossary of Geology* (Bates and Jackson, 1987), we will use the term chromitite strictly for “a rock composed chiefly of the mineral chromite”—i.e., rocks containing >50 modal % chromite. Another process that could affect chromite compositions in plutonic rocks is that, in the case of layered intrusions, there are repeat injections of magma into partly or largely solidified cumulates, which could result in reaction between the injected magma and the cumulates, leading to a change in composition of chromite (Leuthold et al., 2015; Yudovskaya et al., 2019; Marsh et al., 2021).

The Rustenburg Layered Suite of the Bushveld Complex, South Africa, contains 13 to 14 major chromitite layers. These constitute the second-largest Cr resource in the world (U.S. Geological Survey, 2021). Associated with one of these layers, the UG2 is the largest platinum-group element resource (PGE) in the world. The purpose of the current work is to investigate the composition of the chromite and silicate minerals from these layers covering the full stratigraphic section and to consider processes that could have affected the composition of the chromite.

General Geology

The Rustenburg Layered Suite occurs in the northeastern portion of South Africa and is the largest layered intrusion in world (Fig. 1). It was emplaced into the Transvaal Supergroup, which consists of sedimentary and volcanic rocks. Recent high-precision U-Pb zircon age dates from rocks covering the full stratigraphic sequence of the suite cover the range of 2060.12 ± 0.89 to 2054.65 ± 0.42 Ma (Scoates et al., 2021, and references therein). The suite is divided from the base to the top into five zones (South African Committee for Stratigraphy, 1980): the Marginal zone (fine grained norites and gabbro-norites), the Lower zone (predominantly peridotites and orthopyroxenites), the Critical zone (orthopyroxenites, chromitites, norites, and minor anorthosites), the Main zone (gabbro-norites and anorthosites), and the Upper zone (gabbro-norites, magnetites, anorthosites, and diorites) (Fig. 1).

Cousins and Feringa (1964) divided the chromitite layers of the Critical zone into three groups (Fig. 2): the lower group (LG1–7) the middle group (MG1–4), and the upper group (UG1–2). With the exception of the LG4, the chromitite layers

[†]Corresponding author: email, sjbarnes@uqac.ca

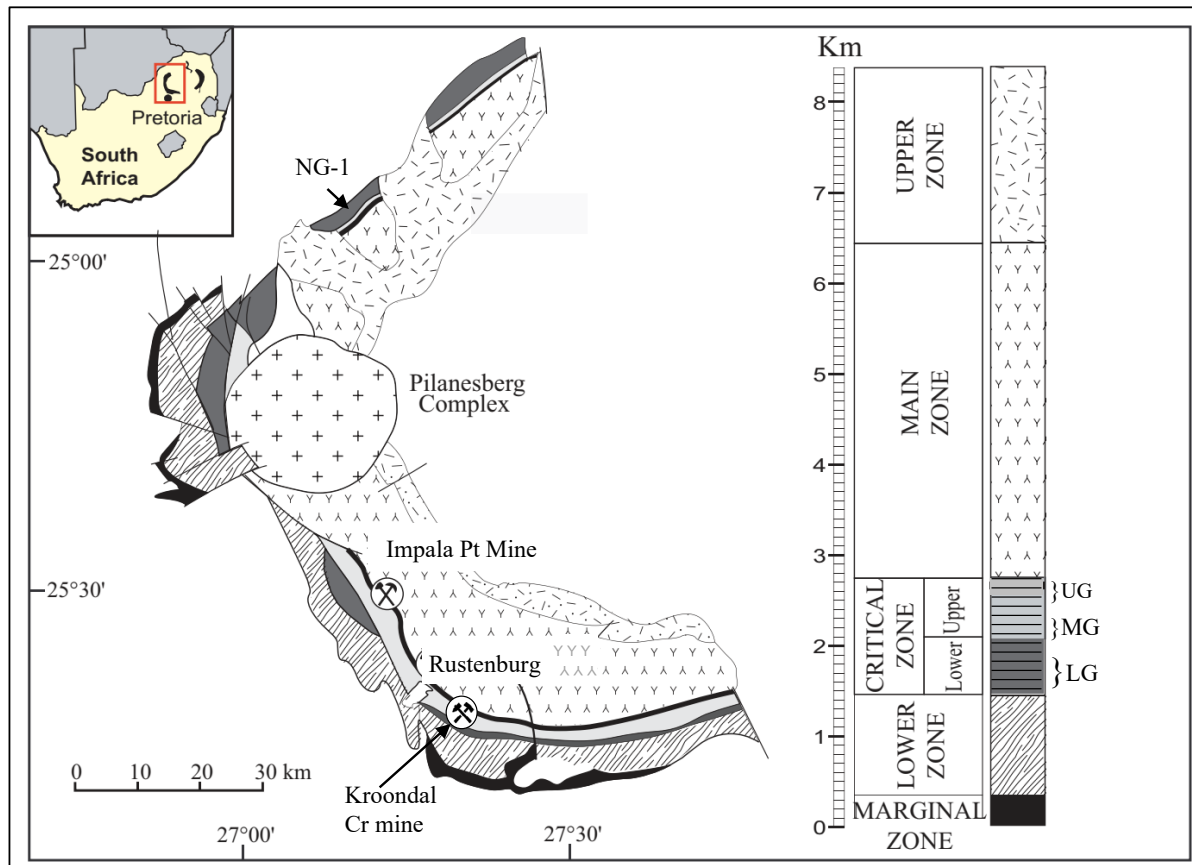


Fig. 1. Map of the western limb of the Bushveld Complex, modified after von Gruenewaldt et al. (1986, 1989), showing the locations of the boreholes used in this study.

LG1 to 7 and MG1 in our study are hosted by orthopyroxenites. The LG4 is associated with harzburgite. The chromitite layers MG2 to UG2 occur toward the base of cyclic units, which consist of orthopyroxenites, norites, and anorthositic. At some other localities, the UG2 is associated with harzburgite. The PGE-rich Merensky reef, which is commonly defined by the presence of two or more thin (1–5 cm) chromite-rich layers, occurs toward the top of the Critical zone.

Using the term “layer,” as in “UG1 layer,” is a little misleading, as it implies a single layer of chromitite is present in each case. In reality, in many cases there is a thick layer of chromitite, with several thinner layers of chromitite both below and above the thick layer. In some cases, complex anastomosing chromitite layers are present—most famously in the case of the UG1 and UG2 layers in the Dwars River area (Voordouw et al., 2009; Pebane and Latypov, 2017).

Materials and Methods

Materials

The LG samples obtained for this study are from the Nooitgedagt borehole (NG1) from the northwestern part of the complex (Fig. 1). Samples from these chromitite layers have been previously studied for their PGE content and for the variations in major element contents of chromite (Teigler, 1990; Teigler and Eales, 1993; Scoon and Teigler, 1994). The MG, UG, and Merensky samples are from the southwestern part of the complex. The MG samples

are from drill core at Kroondal mine (Fig. 1). More details on the mine can be found in Arunachellan (2022). The UG and Merensky samples are from boreholes on the farms Reinkoyalskraal and Vlakfontein, of Impala mines (Fig. 1). A sample of UG2 from the SIE borehole to the northwest of Pretoria (Maier and Bowen, 1996) was also included. The PGE contents and chromite compositions of the rocks from the UG chromitites from the Impala mine have been reported in Maier and Barnes (2008) and Barnes et al. (2023). The PGE content and whole-rock compositions of the Merensky samples are reported in Barnes and Maier (2002) and Mansur and Barnes (2020).

It has been shown that in some cases there are variations in compositions of chromite within a single chromitite layer, which has been attributed to crystal fractionation and/or repeated injection of chromite-bearing magma (Naldrett et al., 2012; Junge et al., 2014; Langa et al., 2021). Bearing this in mind, provided material was available, we took samples across each chromite layer (Fig. 2). Photographs of selected hand specimens are shown in Appendix 1, Figures A1 to A3.

Methods

Orientated polished sections were made of each sample. These were examined with a petrographic microscope, and grains for analysis were selected from the bottom to the top of each section. In samples from the contact with the surrounding silicate rocks, this enabled an investigation of possible interaction of chromite with silicate minerals or liquids derived

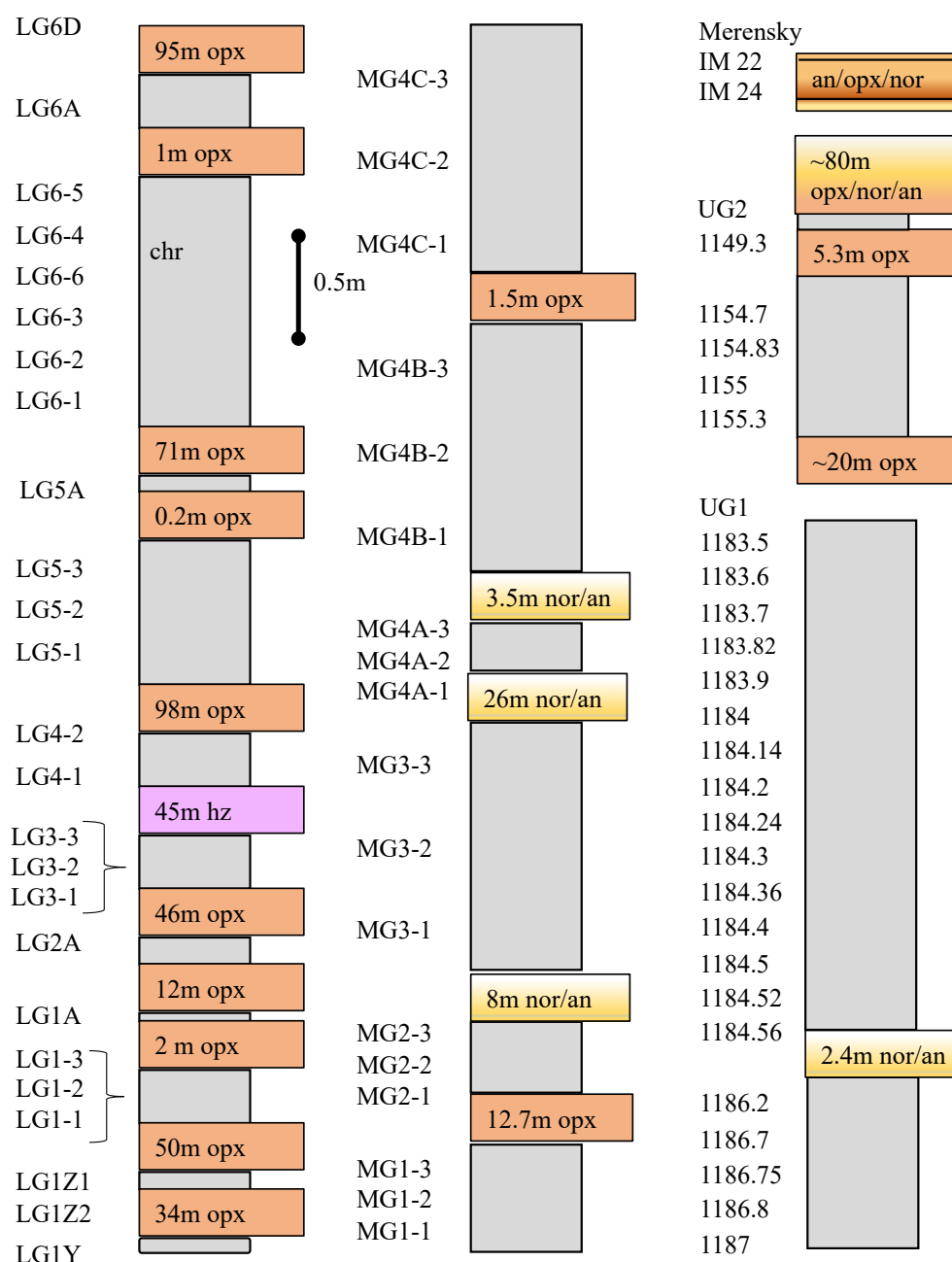


Fig. 2. Position of the samples within each borehole. Abbreviations: an = anorthosite, chr = chromitite, hz = harzburgite, nor = norite, opx = orthopyroxene. Note the scale bar applies only to the chromitite layers.

from the underlying or overlying rocks. In the central part of the chromitite layers, small grains of silicate minerals are present, and three grains of chromite in contact with silicate grains and three not in contact with silicate grains were selected. In total ~700 analyses were collected.

Major elements (Mg, Al, Fe, and Cr) and minor elements (Si, Ti, Mn, and Ni) were determined at the Université Laval, Québec City, with a CAMECA SX100 microprobe by wavelength dispersive spectrometry (beam size 5 μm , accelerating voltage 15 Kev, and current 20 nA). Results for the full data set are reported in Appendix 2, Table A1, and details on analytical conditions and reference materials are listed in Appendix 2, Table A2.

The concentrations of major, minor, and trace elements were determined by laser ablation-inductively coupled plasma-mass spectrometry (LA-ICP-MS) at LabMaTer, Université du Québec, Chicoutimi, using an Excimer 193-nm resolution M-50 laser ablation system coupled with an Agilent 7900 mass spectrometer. The beam size was 44 μm , and line scans were carried out across the grains with a stage speed of 5 or 10 μm depending on the size of the grain. Where the chromite grain was in contact with a silicate mineral, a line scan across the two minerals was collected. This produces a signal consisting of silicate, followed by ~40 to 80 μm of mixed signal followed by a chromite only signal (Fig. 3). The segments of the line covering the silicate and chromite were

reduced separately, and the mixed signal was discarded. Maps of the distribution of the elements were made with essentially the same conditions, except that the beam size was 10 μm and the stage speed was 5 $\mu\text{m/s}$ to provide better resolution but at the expense of sensitivity. Data reduction was carried out using the Iolite package for Igor Pro software (Paton et al., 2011). The full data set of the analyses is reported in Appendix 2, Table A1. Results for reference materials and more details on analytical conditions are reported in Appendix 2, Table A3.

Results from the microprobe are more precise than the laser ablation results for Mg, Al, Si, Cr, and Fe, and these concentrations were used. The results from the LA-ICP-MS analyses for Mg, Al, and Cr were generally within 5 relative % of the microprobe results. The results from the LA-ICP-MS were used for all other elements.

Whole-rock analyses were carried out by LA-ICP-MS of a Li tetraborate bead, which contained 2.25 g of flux powder and between 0.125 and 0.5 g of sample. The ratio of sample to flux was determined by whether all the chromite in the sample was dissolved. The results obtained for the reference materials agree with the working values within analytical error (App. 2, Table A4). More details on the analytical method are reported in Appendix 2, Table A4 and whole-rock analyses in Appendix 2, Table A5.

Results

Petrography

It is well-known that chromite reequilibrates with evolving silicate liquids and with the adjacent silicate minerals after solidification. In addition, chromite grains from chromitite layers show triple junctions with 120° angles at the contacts and tend to be larger than the chromite grains at the margins of the layers or in the silicate host rocks. Textural studies of the UG1 and UG2 attribute these features to textural maturation via the dissolution of smaller crystals and growth of larger crystals possibly in the presence of intergrain melts, (Eales and Reynolds, 1986; Veksler et al., 2018; Hunt et al., 2021). The large grains then coalesced to form dense coarse-grained zones. For these reasons it is important to note the context of the analyzed grains.

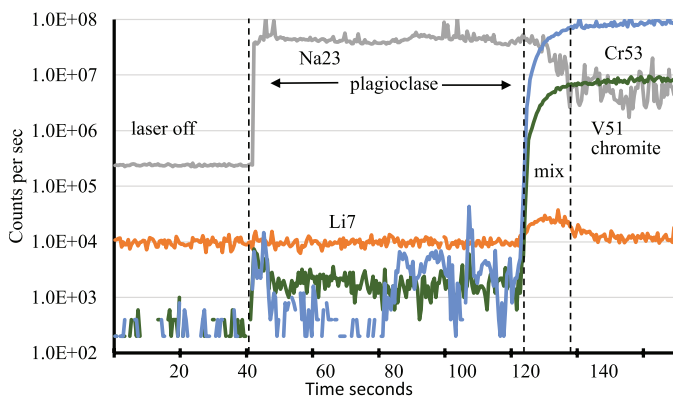


Fig. 3. Traverse across plagioclase into chromite illustrating the separation of the signal into plagioclase and chromite, with increase in Li in the mixed signal part of the traverse.

In the orthopyroxenites, chromite occurs as disseminated small cubes (0.05–0.1 mm diam), in many cases forming chains of grains interstitial to the silicate minerals or included in orthopyroxene. The silicate minerals consist of subhedral orthopyroxene (~90–95 modal %, 3–5 mm in length) with interstitial anhedral plagioclase (~2–10 modal %, 1 mm in length) and phlogopite (<<1 modal %, 1 mm in length) (Fig. 4A). The LG4 harzburgite is poikilitic with orthopyroxene oikocrysts, 1 to 2 cm in size, which include subhedral 1- to 2-mm olivine chadacrysts. Chains of small (0.1–0.2 mm) euhedral chromite grains are present within and among the orthopyroxene oikocrysts (Fig. 4B).

Below some chromitite layers (LG1, LG2A, LG4, LG6, and MG1) there are narrow zones (1–2 cm) of chromite grains in an interconnecting network or matrix surrounding the mafic silicates (Fig. 4C). The chromite grains are euhedral and relatively small (0.1 mm). Above this, some chromitite layers contain patches, which consist of orthopyroxene oikocrysts with chromite chadacrysts surrounded by a dense matrix of chromite grains (Fig. 4D). The chadacrysts are euhedral and are smaller (0.05–0.1 mm) than chromite grains surrounding the oikocryst (0.1–0.5 mm). Where these larger chromite grains (0.1–0.5 mm) are in contact with each other they have triple junctions with 120° angles. Small patches (0.1 mm) of orthopyroxene are also present among the large grains (Fig. 4E). Based on whole-rock Cr_2O_3 concentrations divided by Cr_2O_3 concentrations in chromite, the average chromite content of the LG1 to LG6 is 86 wt %. When we allow for density difference between silicates and oxides, this corresponds to ~79 modal % (App. 2, Table A5).

The MG3, MG4A, MG4B, UG1, and Merensky reef chromitite layers are underlain by norite or anorthosite, whereas the MG1, MG2, and the UG2 chromitite are underlain by orthopyroxenite. Overlying the MG2, MG3, MG4A, MG4C, UG1, and Merensky chromitite layers are norite or anorthosite, whereas the MG1, MG4B, and UG2 are overlain by orthopyroxenite (Fig. 2). Disseminated chromite in the norites and anorthosites shows a similar compartment to chromite in the orthopyroxenite (Fig. 5A, B), but plagioclase in this case is more abundant and takes various forms. It occurs as large (up to 1 cm) oikocrysts enclosing both orthopyroxene and chromite (Fig. 5A) and as subhedral laths 2 to 3 mm in length (Fig. 5B). The boundaries between the chromitite layers and the silicate layers tend to be sharp (Fig. 5A, B). The chromite in the chromitite layers occurs as subhedral chadacrysts with rounded corners, within plagioclase and orthopyroxene oikocrysts 5 to 10 mm in size (Fig. 5C, D). Based on whole-rock analyses, the MG and UG chromitite layers are not as rich in chromite as the LG chromitite layers, containing on average 78 wt % chromite, equivalent to ~69 modal % (App. 2, Table A5).

Both of the chromite-rich layers in the Merensky reef in our samples are narrow, with the lower layer being 2.5 cm wide and the upper layer being 0.5 cm (App. 1, Fig. A3). The lower layer has a sharp contact with the underlying anorthosite. Between the upper and lower seam is a coarse-grained melanorite (usually referred to as a pegmatoidal pyroxenite) with disseminated chromite. Both layers consist of ~20 to 30 modal % chromite with oikocrysts of orthopyroxene and plagioclase (Fig. 6A, B). Chromite occurs in a number of different forms: as small (0.05–0.1 mm)

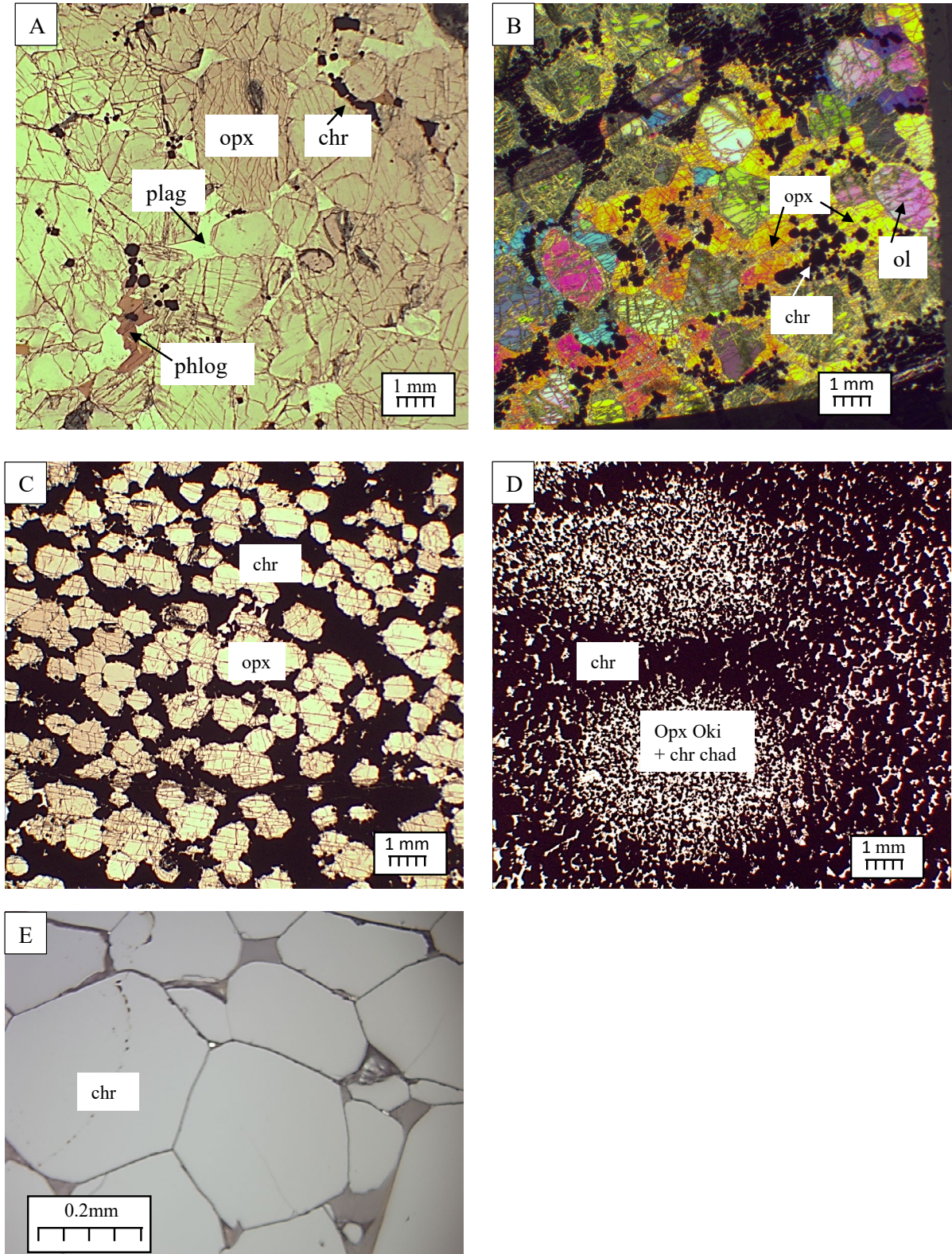


Fig. 4. Photomicrographs of chromite textures in the LG chromites. (A) Orthopyroxenite with disseminated chromite. (B) Chromite and olivine chadacrysts in orthopyroxene oikocrysts. (C) Matrix of chromite chains surrounding orthopyroxene. (D) Patchy textures in chromitite, consisting of small chromite chadacrysts in orthopyroxene surrounded by coarser-grained chromite grains. (E) Chromitite showing triple junctions between chromite grains. Abbreviations: chad = chadacrysts, chr = chromite, Oki = oikocrysts, ol = olivine, opx = orthopyroxene, phlog = phlogopite, plag = plagioclase.

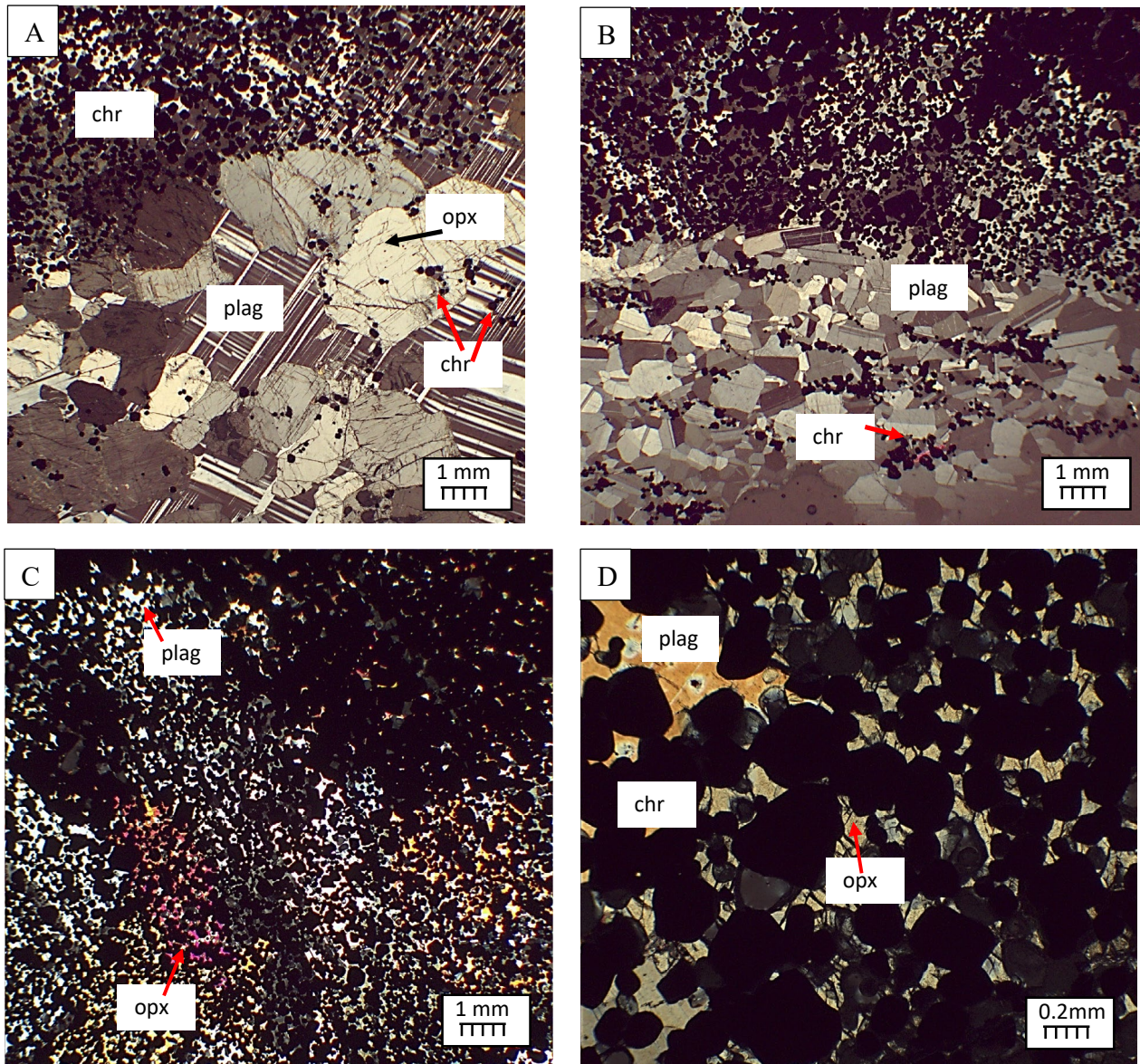


Fig. 5. Photomicrographs of chromite textures in the MG and UG chromitites. (A) Contact between norite and chromitite showing oikocrysts of plagioclase containing chromite and orthopyroxene. (B) Contact between norite and chromitite showing disseminated chromite among the plagioclase laths and larger chromite grains included in plagioclase oikocrysts in the chromite layer. (C, D) Chromitite with subhedral chromite grains in oikocrysts of orthopyroxene and plagioclase. Abbreviations: chr = chromite, opx = orthopyroxene, plag = plagioclase.

cubes enclosed within pyroxene and plagioclase and as larger (0.5–1 mm) blocky grains among the plagioclase and orthopyroxene (Fig. 6A, B). In addition, in the lower layer chromite occurs as amoeboidal (0.5–1 mm) grains (Fig. 6B, C). In many cases the amoeboidal grains contain circular silicate inclusions.

Chromite—major element concentrations

Element maps of chromite grains show that neither the chromite in contact with pyroxene (Fig. 7) nor the chromite in contact with plagioclase (Fig. 8) show compositional zonation at the scale of 10 μm . The chromites are Al chromites (Fig. 9A). The Cr# and Fe# from the chromitite chromites cover ranges similar to those previously reported (shaded

areas on Fig. 9B, C) with the LG chromites having the highest Cr# and lowest Fe# and the UG1 chromites having the lowest Cr# and higher Fe# (selected analyses in Table 1; all analyses in App. 2, Table A1). In their study of chromite-bearing rocks associated with UG2 chromitite from the northern limb, Langa et al. (2021) found that chromites in rocks with less than 40 modal % chromite have higher Fe# than chromites from chromitite. In our study, chromites at the margins of the chromitites, including those that are disseminated, and those that form chains that in rare cases connect to form a matrix or network tend to have higher Fe# than the chromite from adjacent chromitites (Fig. 9B, C). In the text below, chromite in rocks with <50 modal % chromite will be referred to as disseminated chromite.

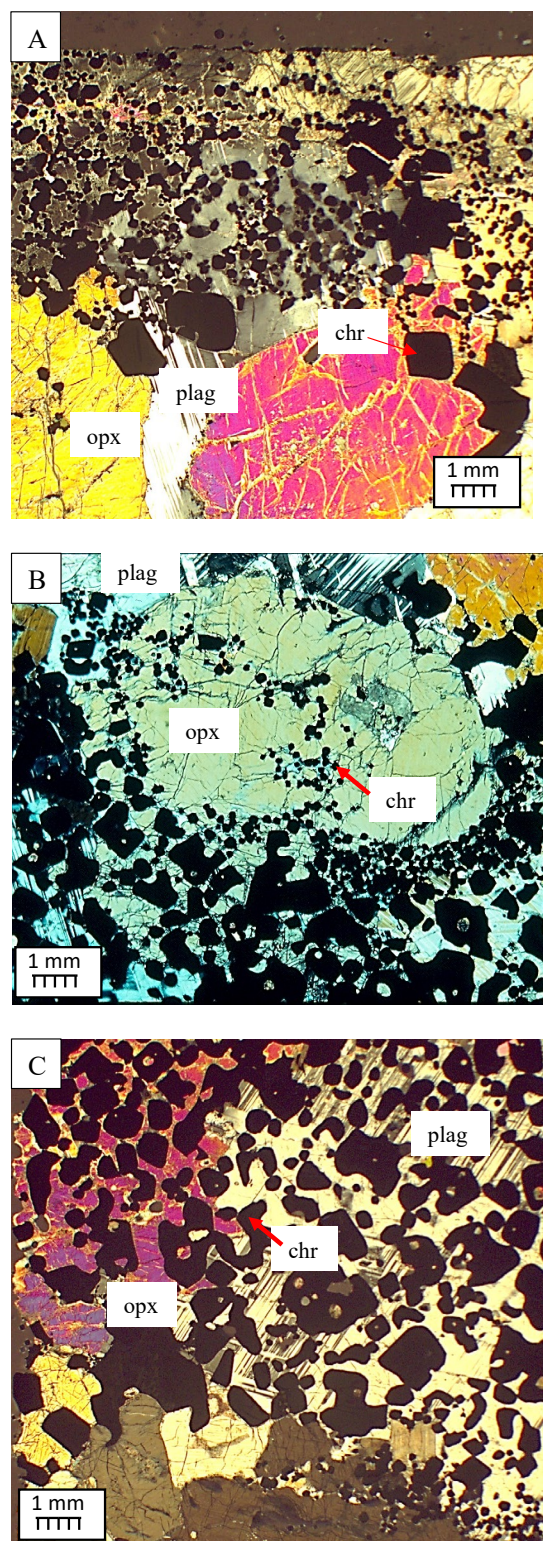


Fig. 6. Photomicrograph of chromite textures from the Merensky reef. (A) Lower contact of upper chromite layer showing small cubic grains in plagioclase and large blocky grains among the silicate grains. (B) Upper contact of lower chromite layer showing small cubic chromite chadacrysts in orthopyroxene and amoeboidal chromite grains within the layer. (C) Center of the lower chromite layer showing amoeboidal grains with round silicate inclusions. Abbreviations: chr = chromite, opx = orthopyroxene, plag = plagioclase.

The Cr_2O_3 concentrations are highest in chromite from the LG chromitites and range from approximately 47 to 53 wt % (Fig. 10A). The Cr_2O_3 concentrations increase up-section from the LG1 to the LG4 and then decrease toward the LG6. The Cr_2O_3 concentrations in chromites from the MG, UG, and the lower Merensky layers vary between 42 to 46 wt % (Fig. 10A). The chromite from the upper Merensky chromite layer and disseminated chromite from between the two Merensky chromite layers contain the least Cr_2O_3 at 38 to 41 wt %.

The Al_2O_3 concentrations of chromites from the LG layers range from approximately 10 to 14 wt % (Fig. 10B), whereas chromite from the MG, UG, and Merensky layers are distinctly more Al_2O_3 rich, from 13 to 19 wt %. Disseminated chromites appear to contain less Al_2O_3 than chromites from the associated chromitite layer. An exception to this is the LG4 layer where the disseminated chromite contains more Al_2O_3 than the chromitite chromite (Figs. 10B, 11A; Table 1; App. Table A1).

The MgO contents of chromite vary from 5 to 12 wt % with the highest values found in the LG4 chromites. The MgO content of the disseminated chromites is lower than that of the chromites of the adjacent chromitite layer (Figs. 10C, 11A).

The $\text{FeO}_{\text{Total (T)}}$ concentrations of chromitite chromite vary from 21 to 29 wt % (Fig. 10D). Disseminated chromites and the chromites from the two Merensky chromite layers show higher values at 29 to 43 wt % (Fig. 10D). The FeO_T content of the disseminated chromites is higher than that of the chromite of the adjacent chromitite layer (Figs. 10D, 11A). $\text{Fe}^{3+}/\text{Fe}_{\text{Total (T)}}$ values are generally between 0.2 and 0.3, with the UG1 chromites showing the lowest values and chromites from the upper Merensky layer showing the highest values (Fig. 10E). There is no difference in $\text{Fe}^{3+}/\text{Fe}_T$ of disseminated chromite and chromitite chromite from the adjacent layer (Figs. 10E, 11A).

Despite the fact that some chromites within chromitite layers are in contact with silicate minerals and in some cases are chadacrysts, the compositions of chromites from within any particular chromitite layer are similar (Figs. 10, 11B; App. 2, Table A1).

PGEs and Au

The samples investigated in this study have been shown to be enriched in Os, Ir, Ru (the iridium subgroup PGEs [IPGEs]), and Rh and in the case of the UG samples, in Pd, Pt, and Au (Teigler and Eales, 1993; Scoon and Teigler, 1994; Barnes and Maier, 2002; Maier and Barnes, 2008). This is the case for most chromitites from the Bushveld Complex (von Gruenewaldt et al., 1986; Naldrett et al., 2009, 2012). Thus, it is important to consider whether any of these elements are present in chromite. Chromite from the marginal sills of the Bushveld Complex contain detectable levels of IPGEs and Rh and Pt, Pd, and Au below detection levels (Pagé and Barnes 2016; App. 2, Table A1). However, only low levels (in many cases below detection levels) of PGEs have been reported for chromite grains from the LG6, UG2, and Merensky reef (Park et al., 2012; Pagé and Barnes, 2016; App. 2, Table A1). Furthermore, PGE and Au concentrations for all chromite grains in the current study are below the detection limits (Table 1; App. 2, Table A1). Given the presence of laurite and other platinum group minerals in our samples (Maier et al.,

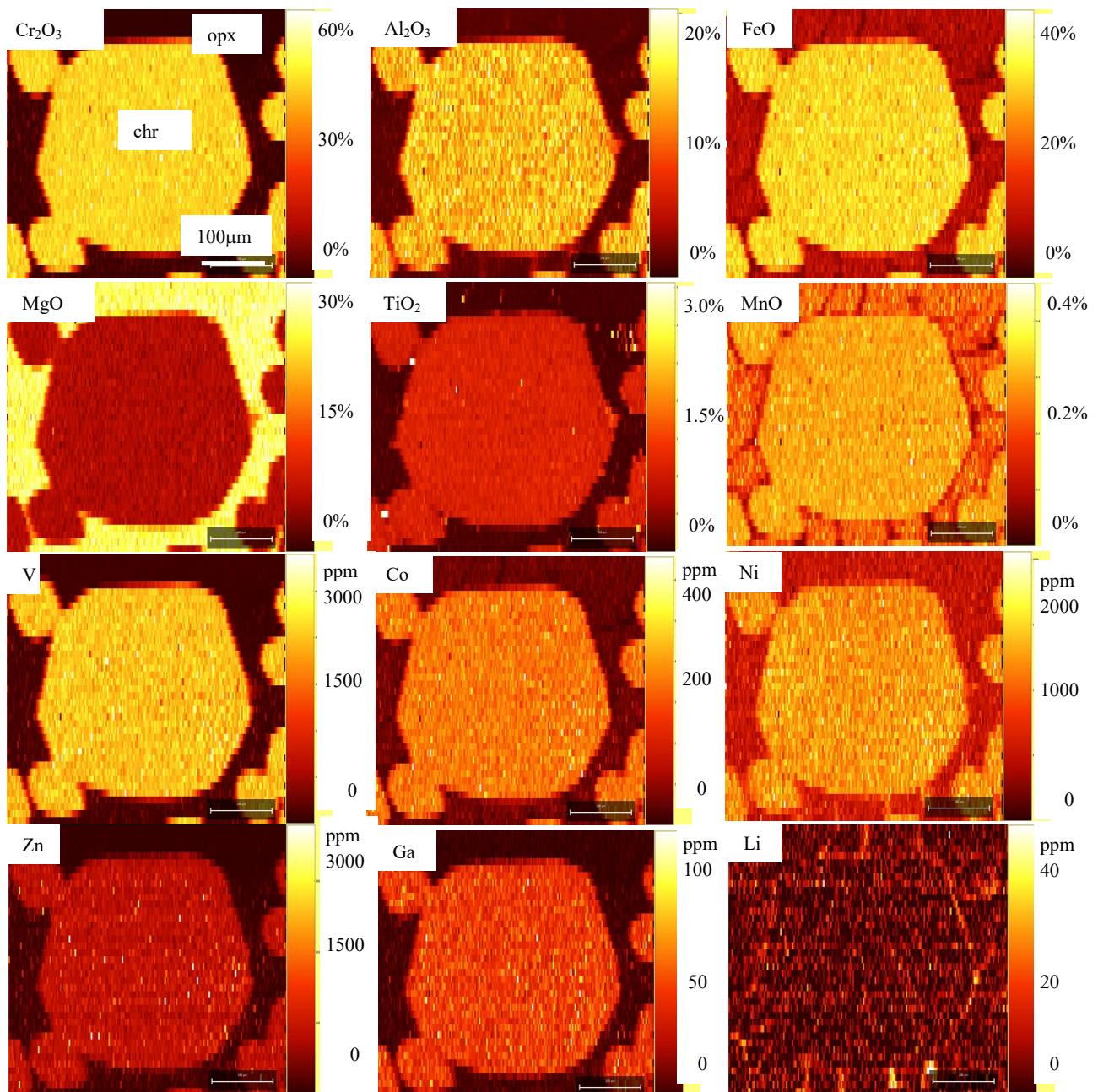


Fig. 7. Element maps of chromite chadacrysts in orthopyroxene oikocrysts from the UG2 (sample SIE 197). Note the chromite does not show compositional zoning. Abbreviations: chr = chromite, opx = orthopyroxene.

1999; Prichard et al., 2004) and as reported from other chromite-rich rocks in the Bushveld (Osbaahr et al., 2014; Junge et al., 2016; Oberthür et al., 2016; Kaufmann et al., 2019), the hosts of most the PGEs would appear to be platinum group minerals.

Concentrations of minor elements Ti, V, Mn, Co, Ni, and Zn

The Ti contents of the chromitite chromites from the LG to UG2 layers increase from approximately 2,500 ppm in the LG layers to 6,000 ppm in the MG and UG layers. Many of the disseminated chromites show similar concentrations, but some are richer in Ti (Figs. 11A, 12A; Table 1; App. 2, Table A1). The chromites from the Merensky reef chromite

layers contain the highest Ti values at approximately 7,000 to 12,000 ppm, with the upper layer containing the most Ti.

A potential complication in interpreting the Ti concentrations in chromite is the presence of rutile. Rutile in chromites from the Bushveld has been investigated by Ver Hoeve et al. (2018), who concluded that the rutile inclusions in chromite formed by exsolution from chromite and thus are part of the original composition of the chromite. Rutile inclusions are present in some of the Merensky chromites in our study (App. 1, Fig. A4) but are in most cases too small (1–10 µm) to be distinguished in laser spectrum and have therefore been integrated with the signal. Furthermore, the Ti content of our chromite as determined by microprobe and by LA-ICP-

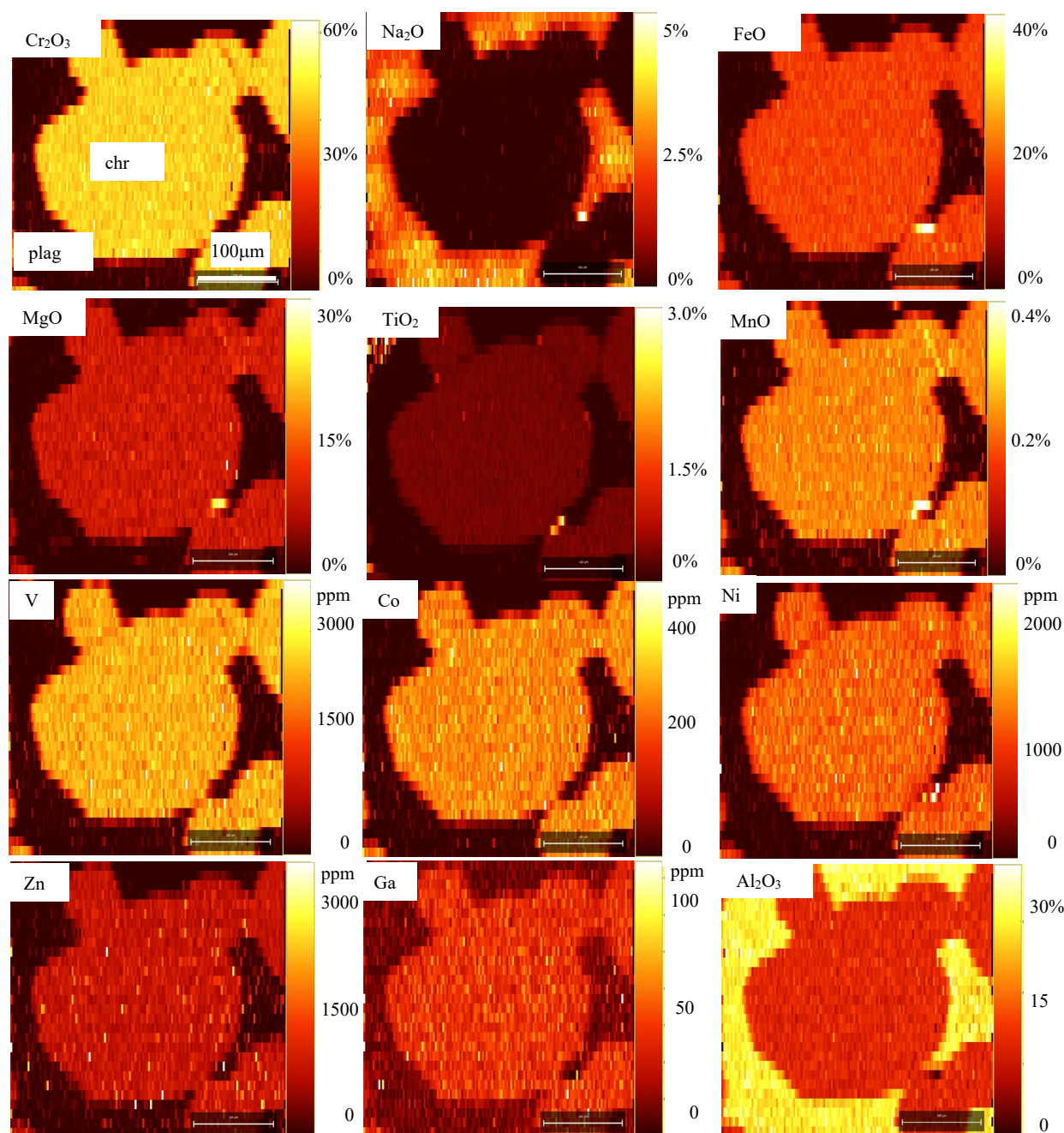


Fig. 8. Element maps of chromite chadacrysts in plagioclase oikocrysts from the UG2 (sample SIE 197). Note the chromite does not show compositional zoning. The plagioclase shows reverse compositional zoning as illustrated by the variation in Na_2O content. Abbreviations: chr = chromite, plag = plagioclase.

MS agree to within 5 relative %, and thus the integration of the small rutile inclusions in the LA-ICP-MS signal does not change the estimated Ti concentration in chromite. However, enrichment in Ti in the time resolved analyses (TRA) spectrum was observed in a few Merensky chromite grains, and these parts of the LA-ICP-MS signals are also enriched in Y, Zr, Nb, Sn, Hf, and Ta relative to the enclosing chromite (App. 2, Table A1). Ver Hoeve et al. (2018) report that rutile is enriched in these elements; thus, these parts of the spectra are probably a mixture of chromite and larger rutile exsolutions.

Vanadium concentrations are lowest in chromites from the LG chromitites at approximately 1,200 ppm and rise to approximately 3,200 ppm in chromites of the UG chromitites. The LG6 chromites are richer in V than the general trend, rising to 3,500 ppm. The disseminated chromite from the Merensky melanorite contains the most V at 4,000 ppm. (Fig. 12B; App. 2, Table A1).

Concentrations of Mn in the chromitite chromites range from 1,500 ppm in the UG1 to a high of ~2,200 ppm in the MG chromite (Fig. 12C). The disseminated chromites contain more Mn than chromites in the adjacent chromitite layer

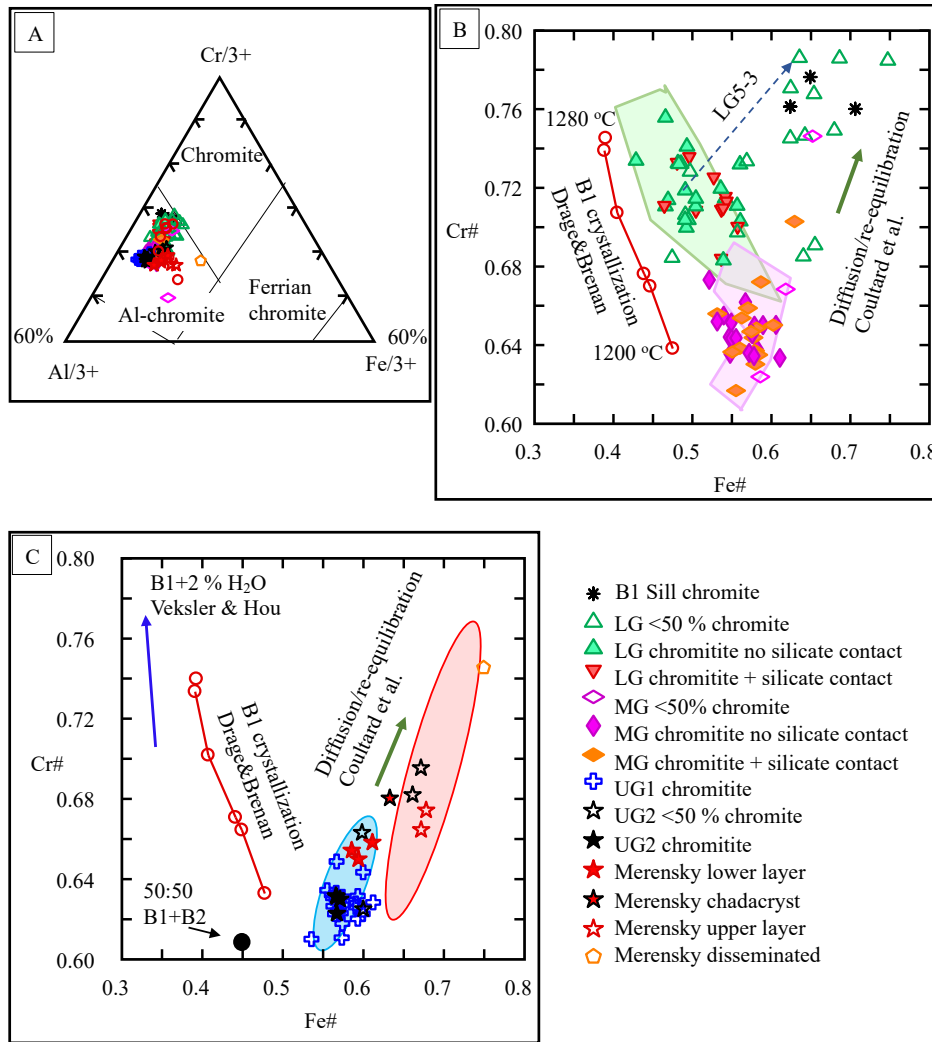


Fig. 9. (A) Classification of the chromite, showing that all of the chromites are Al chromites. (B) Cr# versus Fe# of disseminated and chromitite chromite from LG and MG chromitites; shaded field shows composition of chromite from chromitites as reported from the literature (Naldrett et al., 2012). (C) Cr# versus Fe# of disseminated and chromitite chromite from the UG1 and UG2 chromitites and Merensky reef chromite layers; shaded field shows composition of chromite from chromitites as reported from the literature (Naldrett et al., 2009; Vukmanovic et al., 2013; Scoon and Costin, 2018; Langa et al., 2021). Also shown are the evolution of chromite composition as the B1 magma crystallized (Drage and Brennan, 2023), the trend for chromite compositions when water is added to the B1 magma (Veksler and Hou, 2020), and the trend for reequilibration with a fractionated liquid (Coulthard et al., 2021).

(Figs. 11A, 12C), with the highest concentrations associated with the LG layers at 2,600 ppm. Cobalt concentrations in chromite show a similar distribution. Concentrations vary from a low of 270 to 370 ppm in chromitite chromite and are generally higher in disseminated chromite—between 300 and 560 ppm (Fig. 12D). Concentrations of Ni in chromite, both from chromitite layers and disseminated chromite, increase with increasing height, from ~900 ppm in the LG1 layer to 1,200 ppm in chromite from the UG2 chromitite layer. There is an abrupt increase in Ni concentrations in chromite from the Merensky reef chromite layers, where the chromite contains up to 2,800 ppm Ni (Fig. 12E). In contrast to Mn, Co, and Ni, Zn concentrations are more erratic. Zinc concentrations in chromite from the LG1 to LG4 chromitites are ~500 ppm and show a sudden increase in chromite from the LG5 to the Merensky reef chromite layers at ~700 ppm (Fig. 12F). Some

disseminated chromites are enriched in Zn, with values up to 1,200 ppm, but some are depleted.

Concentrations of trace elements Ga, Sc, Cu, Hf, and Sn

The concentrations of Ga in chromite from the LG chromitite layers are in the range 35 to 45 ppm. The concentrations of Ga in chromites from the MG, UG chromitites and the Merensky chromite layers are higher—50 to 70 ppm (Fig. 13A). Concentrations of Ga in disseminated chromite are similar to the Ga concentrations in chromite from the adjacent chromitite layer (Fig. 11A).

Scandium and Cu concentrations in chromite range from 1 to 14 ppm. There appears to be no relationship between stratigraphic height and the concentrations of these elements in chromite. The disseminated chromite contains lower concentrations of both elements than the chromite from the

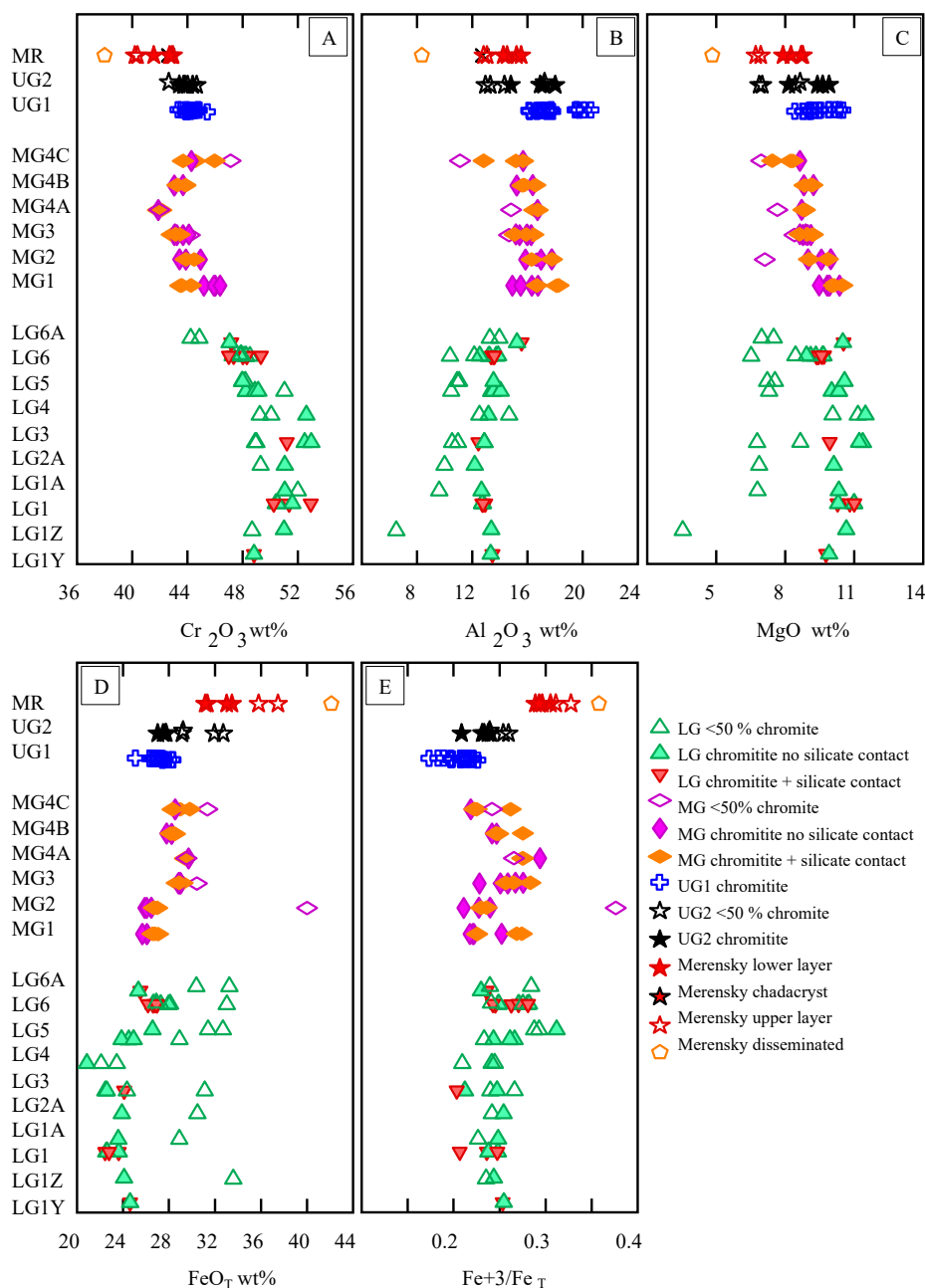


Fig. 10. Variations in concentrations of (A) Cr₂O₃, (B) Al₂O₃, (C) MgO, and (D) FeO_T, and in (E) Fe³⁺/Fe_T ratio with stratigraphic height.

nearest chromitite layer (Figs. 11A, 13B, C). Concentrations of Hf in chromite range from 0.01 to 1 ppm (Fig. 13D), with lowest values in chromite from the LG chromitite layer and the highest in chromites from the MG chromitite layers. Disseminated chromites contain lower concentrations than chromitite chromites (Fig. 11A). Tin and Mo concentrations range from less than method detection limits (0.03 ppm) to 1 ppm, with no clear relationship with stratigraphic height (Fig. 13E, F).

The concentrations of Li in chromite range from 0.25 to 2 ppm (App. 2, Table A1). There does not appear to be a correlation with stratigraphic height. The concentration of Li in disseminated chromite is slightly higher than in chromite from

the nearest chromitite layer. Zirconium and Nb concentrations in chromite range from below detection level to 3 ppm. However, given the possible interference from Cr, these values should be treated with caution. Tantalum concentrations are close to detection level and Ge, As, Y, In, Cd, W, and Re concentrations are below detection levels (App. 2, Table A1).

Variations across individual layers

In the current study, sampling was carried across each chromitite layer, and in most cases three samples (top, middle, and bottom) were selected. No systematic compositional variations within the layers were observed. More detailed sampling was possible across the 1-m-thick LG6 layer, and six samples were

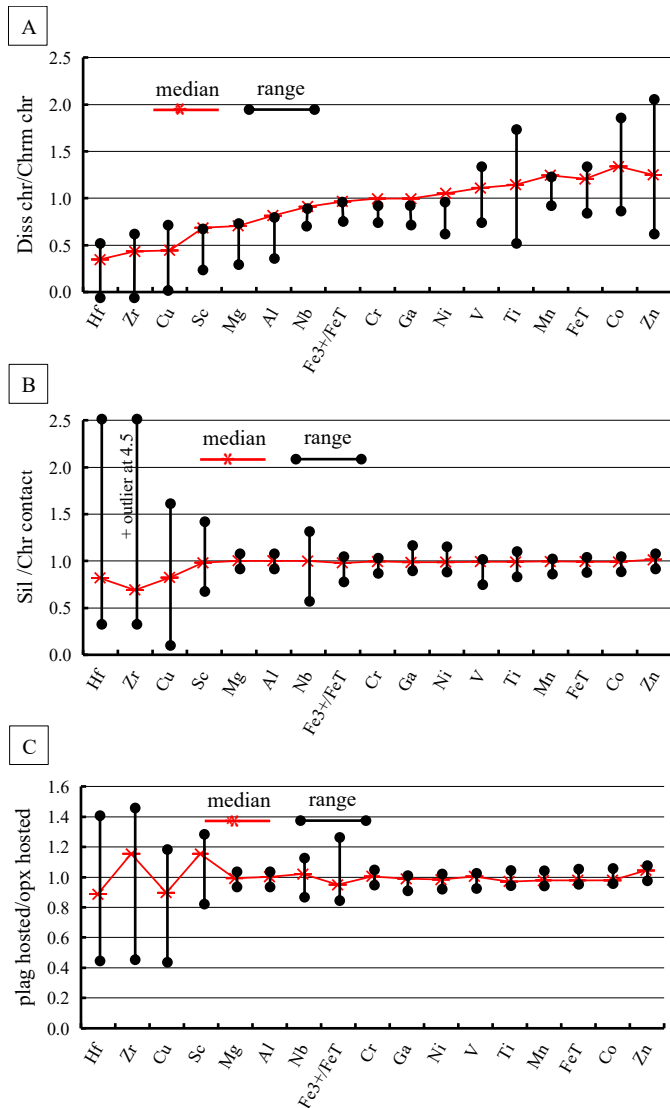


Fig. 11. Concentrations of elements in (A) Disseminated chromite divided by chromite from chromitite. (B) Chromite from chromitite with silicate contacts divided by chromite with no silicate contacts. (C) Chromite in plagioclase oikocrysts divided by chromite in orthopyroxene oikocrysts. Abbreviations: Chr = chromite, Chrm chr = chromitite chromite, Diss chr = disseminated chromite, Opx = orthopyroxene, Plag = plagioclase, Sil = silicate.

obtained. No systematic variation in chromite composition with stratigraphic height is observed within the layer (Fig. 14).

Compositions of the silicate minerals

The compositions of orthopyroxene and plagioclase in contact with chromite were determined in order to evaluate the degree of reequilibration between chromite and the minerals with which it is in contact. For this reason, the focus is on the elements that are present in chromite. In a few cases the silicate mineral in contact with the chromite was clinopyroxene, K-feldspar, or phlogopite. The results for these are listed at the end of Appendix 2, Table A6, and will not be discussed further. Silicate mineral data were not systematically collected from the UG1 and UG2 chromitites, as at the time of that

study (Barnes et al., 2023) as we did not fully appreciate the effects of reequilibration on chromite composition.

Silicate minerals—major elements

The range in Mg# of orthopyroxene is 0.83 to 0.91 (App. 2, Table A6), with the Mg# of the orthopyroxene from the chromite layers tending to be higher than the Mg# of orthopyroxene in the host silicate rocks. This point has been previously noted (Veksler et al., 2018; Tang et al., 2023) and is attributed to reaction between the chromite and orthopyroxene, with the high chromite to silicate ratio in the chromitite layers resulting in a higher Mg# in orthopyroxene than in the host rocks.

The average An# of plagioclase (where An = anorthite) in the LG to MG2 chromitite layers is 0.67 with a range of 0.64 to 0.72 (App. 2, Table A6). The average An# value of plagioclase from the MG3 to UG1 layers is 0.73 with a range of 0.69 to 0.77. The range in Merensky reef chromite layers is 0.72 to 0.77.

The composition of plagioclase from a limited data set from the UG2 chromitite covers a similar range, from 0.63 to 0.72. The UG2 sample from the SIE drill core shows a strong reverse zonation as illustrated by the variation in Na content (Fig. 8; App. 2, Table A6). The plagioclase in contact with chromite is richer in anorthite (An 0.72) than the plagioclase at the core of the plagioclase grains (An 0.63). Reverse zoning of plagioclase has been observed in the Merensky reef plagioclase (Hayes et al., 2025; Smith et al., 2025) and in other silicate rocks of the Critical Zone (Maier and Eales, 1997; Scoon and Costin, 2018; Maier et al., 2021; Latypov et al., 2024). Reverse zonation was not observed in plagioclase of the LG and MG chromitite layers, but as the data were not gathered with this in mind more detailed study would be necessary to firmly establish this point.

Silicate minerals—minor and trace elements

The transition elements (Ti, V, Mn, Co, Ni, and Zn) are concentrated in orthopyroxene with only low levels of these elements present in plagioclase (Fig. 15A-E; App. 2, Table A6). With the exception of Zn (not shown) there are strong positive correlations between the concentrations of transition elements in orthopyroxene and chromite (Fig. 15A-E). Vanadium shows the strongest preference for chromite, with an average calculated apparent partition coefficient between chromite and orthopyroxene of 24. The average partition coefficients between chromite and orthopyroxene for Ti and Co are 6.9 and 6.4, respectively (Fig. 15B, C). Nickel and Mn show a moderate preference for chromite with partition coefficients of 2 and 1.4, respectively (Fig. 15D, E). Pyroxene in contact with disseminated chromite tends to have higher concentrations of Co and Mn. This distinction is not clear for Ti and V.

Scandium shows a strong preference for orthopyroxene (20–70 ppm) with an average partition coefficient of 6.7 between orthopyroxene and chromite (Fig. 16A). Scandium concentrations in plagioclase are close to detection levels.

Of the silicate minerals plagioclase is richest in Ga (12–24 ppm), with only low levels present in orthopyroxene and olivine (<3 ppm; Fig. 16B; App. 2, Table A6). Gallium concentrations in plagioclase are lowest and fairly uniform in the LG and MG layers and highest in the UG2 and Merensky reef. Gallium concentrations are higher in chromite than in

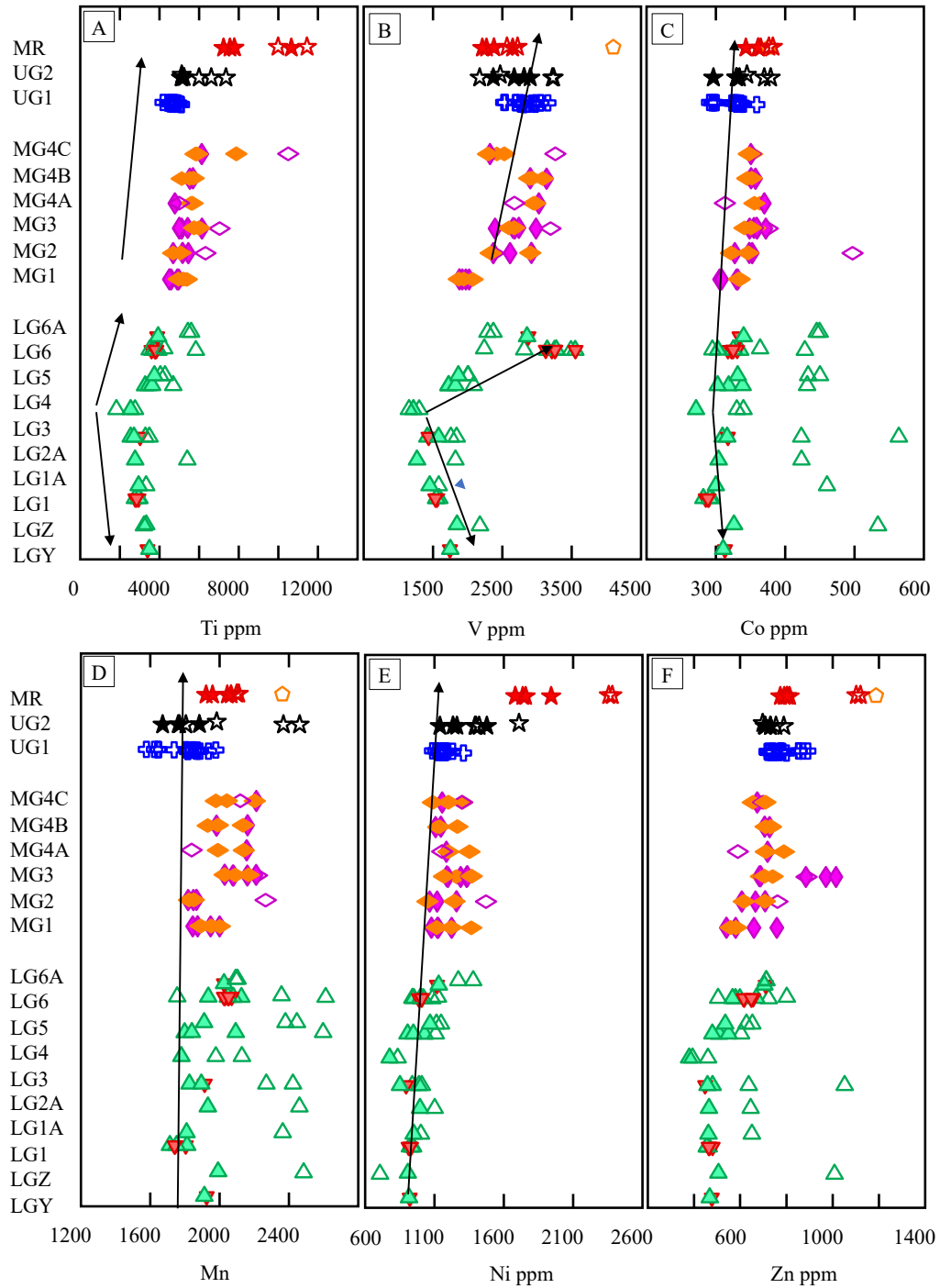


Fig. 12. Variations in concentrations of (A) Ti, (B) V, (C) Co, (D) Mn, (E) Ni, and (F) Zn with stratigraphic height. Legend as on Figure 10. Black lines model concentrations during crystal fractionation.

plagioclase, with an average apparent partition coefficient of 3.7 between chromite and plagioclase.

Discussion

Effects of postcumulus processes

One might expect that smaller cubic chromite grains within the chromitite layers (which in many cases are in contact with

silicates and in some cases are enclosed in oikocrysts) to have a different composition from the larger grains, which appear to be in contact only with other chromite grains. However, this is not the case. All of the chromites from a particular chromitite layer have similar compositions (Figs. 10, 11B, 12, 13; App. 2, Table A1). The difference in concentrations of an element in the chromites in contact with silicate minerals versus concentrations in chromites with no apparent contacts with silicate

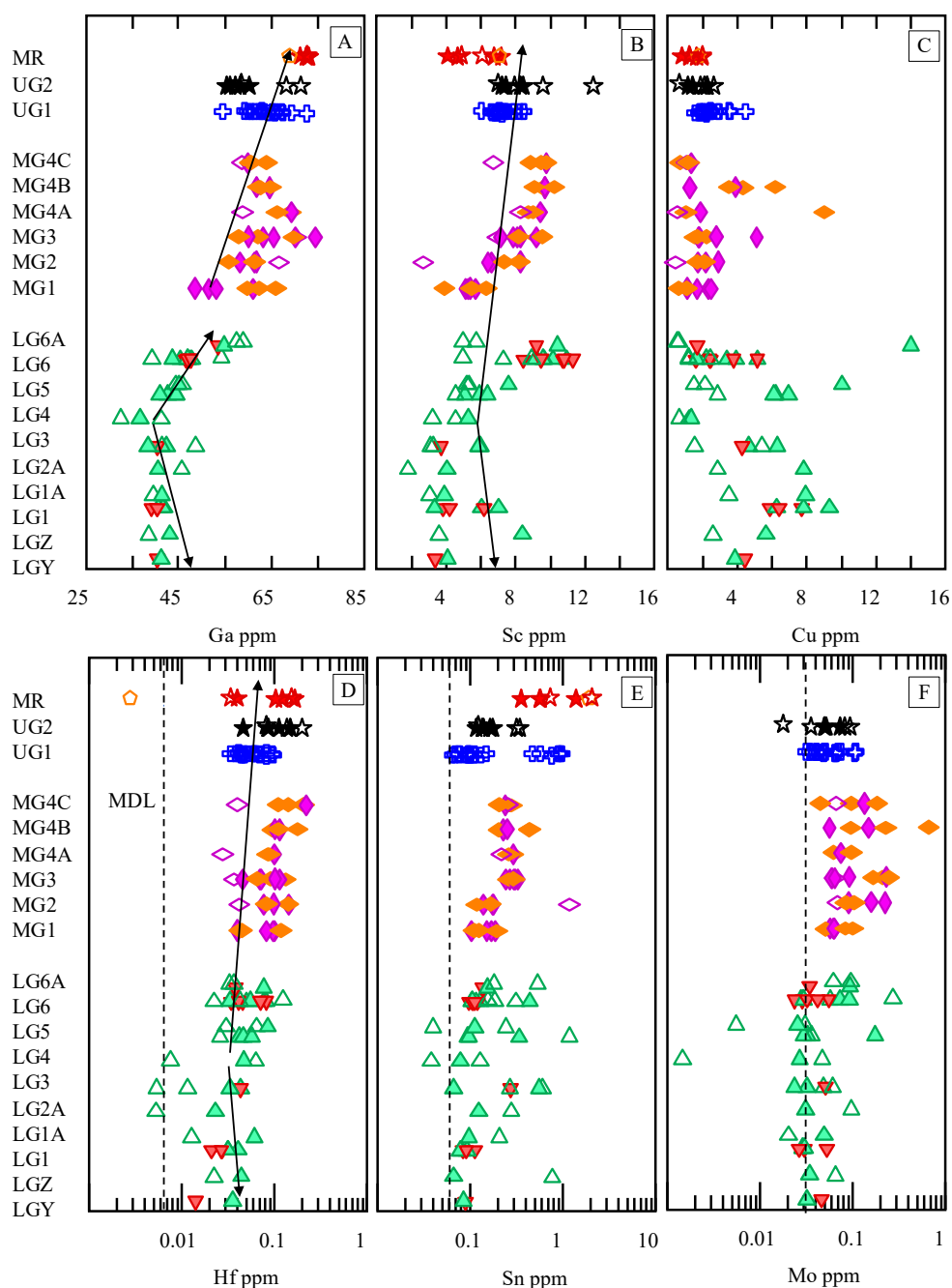


Fig. 13. Variations in concentrations of (A) Ga, (B) Sc, (C) Cu, (D) Hf, (E) Sn, and (F) Mo with stratigraphic height. Legend as in Figure 10. Black lines model concentrations during crystal fractionation.

minerals can be assessed by dividing the concentration of the element in chromite with silicate contacts by the concentration of the element in the chromite with no apparent silicate contacts. The ratio is close to 1 for most elements (Fig. 11B). It does not appear to matter whether the contact mineral is orthopyroxene or plagioclase. In a few cases data are available from the same sample with chromite in contact with orthopyroxene and chromite in contact with plagioclase, and the chromite from each is close to the same composition (Fig. 11C).

The similarity in compositions of all chromite morphologies from within a particular layer could be the result of textural

maturation. The textures in the chromite layers have been studied in detail in the MG2, LG6, UG1, and UG2 chromites (Veksler et al., 2018; Kaufmann et al., 2019; Hunt et al., 2021; Holness et al., 2023; Tang et al., 2023) and are interpreted to indicate that the large grains with triple junctions formed by dissolution of small grains and redeposition on larger grains. This raises the question of how the small grains within oikocrysts could have the same composition as the large grains outside of the oikocrysts. Possibly, the chromite in the oikocrysts was in contact with the interstitial liquid in the third dimension. Also, many oikocrysts contain

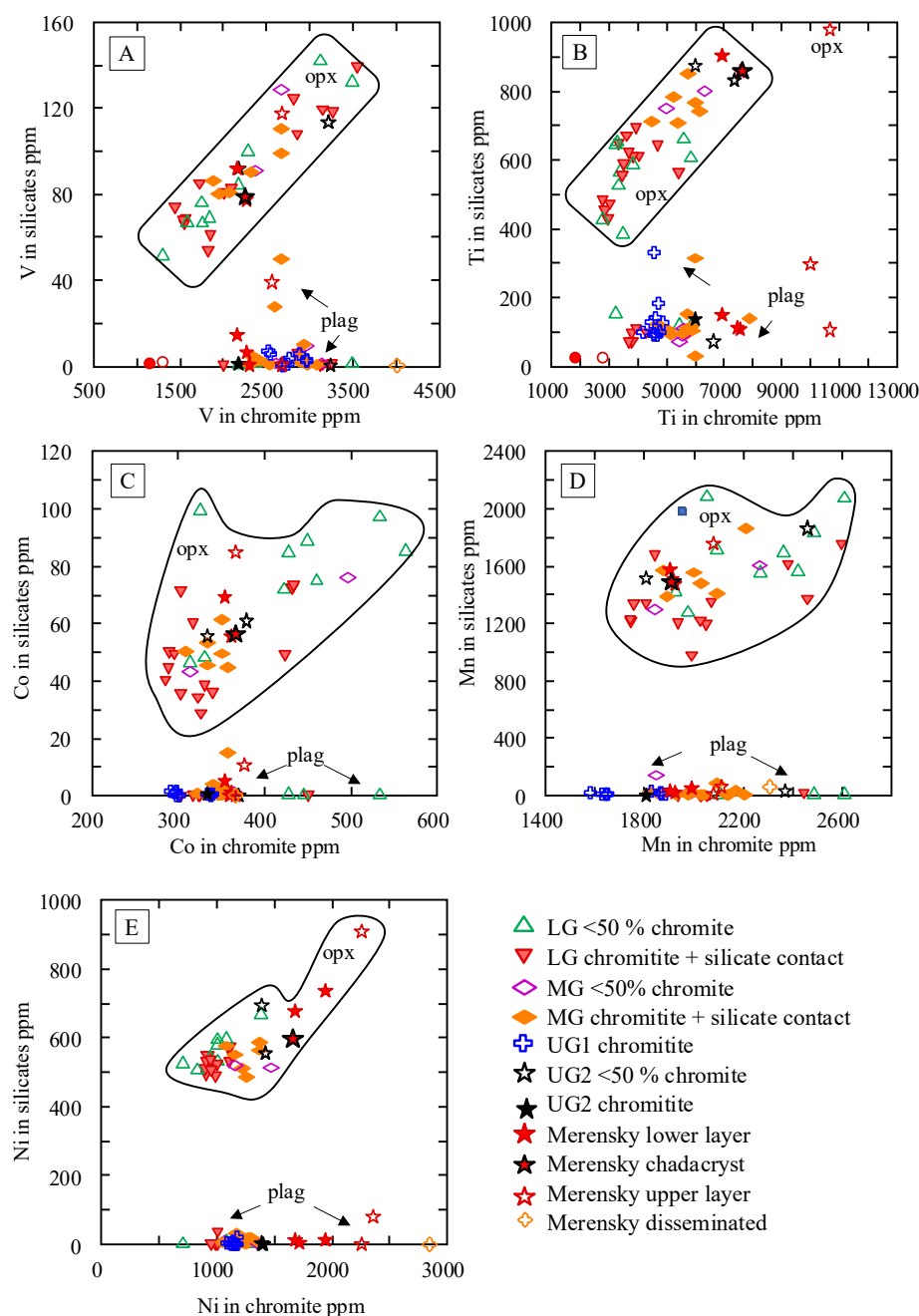


Fig. 14. Concentrations of (A) V, (B) Ti, (C) Co, (D) Mn, and (E) Ni in orthopyroxene and plagioclase versus concentrations in chromite showing the preference of these elements for chromite over orthopyroxene and for orthopyroxene over plagioclase. Abbreviations: opx = orthopyroxene, plag = plagioclase.

fractures, and possibly the chromite and liquid equilibrated through the cracks. It seems that during textural maturation the composition of all the chromite grains have homogenized, and the present composition of the chromite grains in the chromitite layers represents an average of initial and final chromite compositions.

Both the Fe# and Cr# of disseminated chromite are higher than those of the adjacent chromitite layer as illustrated by the line connecting disseminated chromite and chromitite chromite from the same layer for example sample LG5-3 (Fig. 9B). Furthermore, the disseminated chromites are depleted

in Hf, Sc, Cu, Al, and Mg and enriched in Ti, V, Mn, Co, and Zn (Figs. 10, 11A, 12, 13). Gallium, Cr, and Ni concentrations and Fe^{3+}/Fe_T ratios are similar (Figs 10, 11A, 12, 13). These differences in composition are the product of both super- and subsolidus processes, as will be outlined below.

The Cr_2O_3 content of chromite is strongly dependent on f_{O_2} (Barnes, 1986; Murck and Campbell, 1986; Hill and Roeder, 1974), and if the disseminated chromite equilibrated with a more oxidized magma than the chromitite chromite, then the Cr# would be higher. However, the Fe^{3+}/Fe_T ratios of the disseminated chromite are not higher than those of the chro-

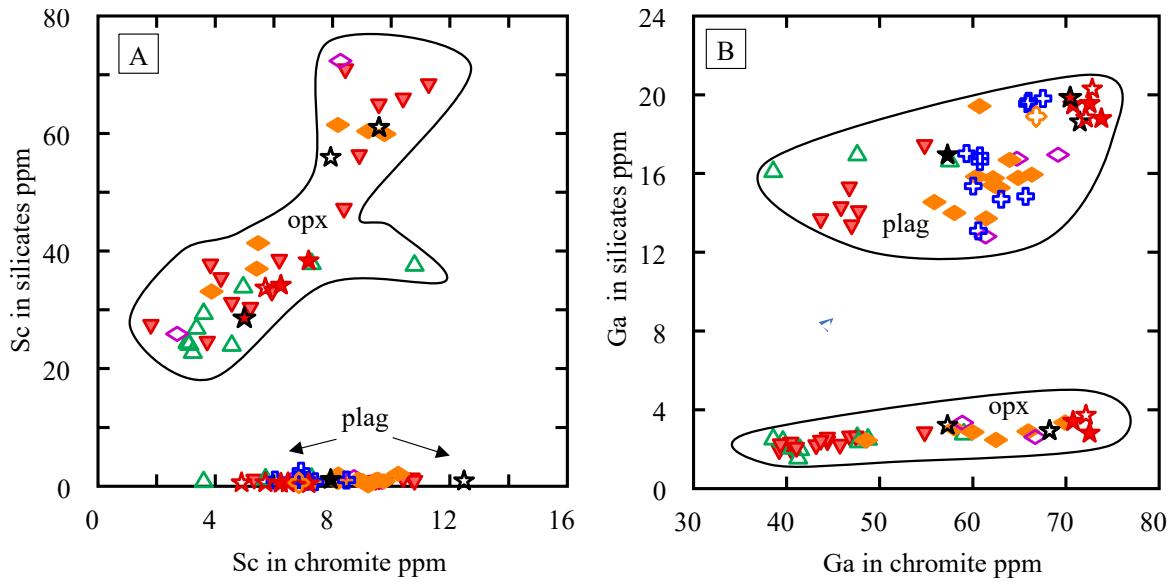


Fig. 15. Concentrations of (A) Sc and (B) Ga in orthopyroxene and plagioclase versus concentrations in chromite showing the preference of Sc for orthopyroxene over chromite and for chromite over plagioclase and the preference of Ga for chromite over plagioclase and for plagioclase over orthopyroxene. Legend as in Figure 14. Abbreviations: opx = orthopyroxene, plag = plagioclase.

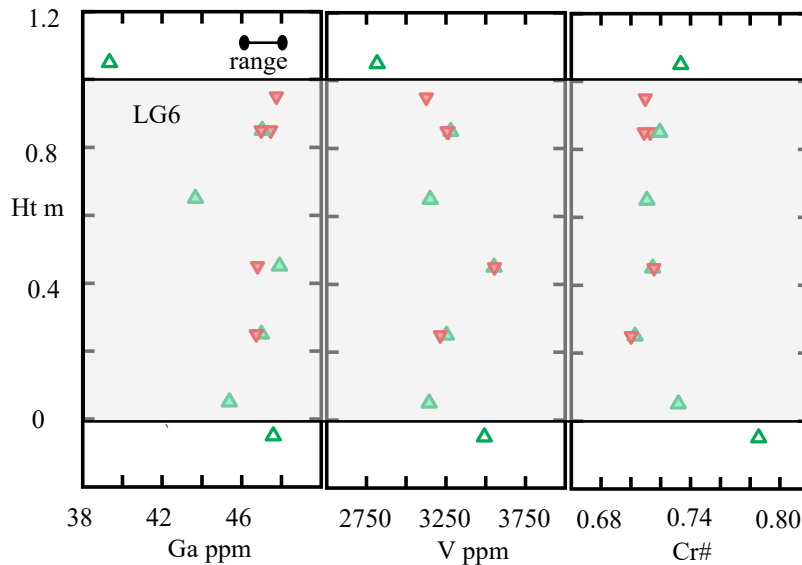


Fig. 16. Variations in Ga and V concentrations and in Cr# of chromite with stratigraphic height across the LG6 layer. Note that the composition of the chromite within the layer does not change. Legend as in Figure 10.

mitite chromite (Figs, 10E, 11A), although they would be if the f_{O_2} had increased. Furthermore, as discussed below, the partition coefficient for V into chromite is also dependent on f_{O_2} and decreases with increasing f_{O_2} ; therefore, the disseminated chromite should contain lower V concentrations than the chromitite chromite, if f_{O_2} had increased, which is not the case (Figs. 11A, 12B). Thus, the increase in Cr# is not due to a change in f_{O_2} .

Chromitite layers are found at the base of cyclic units and are thought to be associated with injections of new magma. After collection of chromite on the cumulate pile, some chromite grains could have settled into the underlying cumulate mush

and reequilibrated with the interstitial liquid, which would have been more fractionated than the newly injected magma. If the chromite settled into the underlying cumulate, then it would have reequilibrated with the fractionated melt. In order to understand how the reaction between chromite and melt affects the composition of chromite, Coulthard et al. (2021) carried out experiments to document the diffusion rates of different elements during reaction of chromite with a boninitic melt. They found that the 2+ ions Fe^{2+} and Mg^{2+} rapidly equilibrated with the liquid. Diffusion of the 3+ ions was slower than the 2+ ions, and the order of diffusion for 3+ ions was as follows: Fe^{3+} faster than Al^{3+} , which was faster than Cr^{3+} . This is agree-

ment with interdiffusion coefficients for Cr and Al determined by Suzuki et al. (2008), who found that diffusion of Al is an order of magnitude higher than Cr. As a result, both Cr# and Fe# increased as the chromite reacted with the melt (Fig. 9B, C). In the case of the Bushveld chromite, it is clear that the disseminated chromite is depleted in Al relative to the chromitite chromite, whereas the Cr concentrations are the same (Figs. 10A, 11A). Thus, the high Cr# in disseminated chromite may reflect reequilibration and faster diffusion of Al into the melt than Cr, as suggested by Coulthard et al. (2021).

Diffusion of Al into the fractionated melt requires that this melt be depleted in Al relative to the newly injected melt. This requires that the fractionated melt was crystallizing plagioclase. The Lower zone and Lower Critical zone of the Bushveld have been proposed to have crystallized from a Mg-rich basaltic andesite, known as the B1 (Harmer and Sharpe, 1985; Barnes et al., 2010; Godel et al., 2011). Modelling of the crystallization of the B1 magma using MELTS (Rhyolite v1.02.2, Ghiorso and Gualda, 2015) indicates that plagioclase appears on the liquidus at $\sim 1,150^\circ\text{C}$. Based on the Al-in-olivine geothermometer (Coogan et al., 2014) the LG4 chromite and olivine equilibrated between $1,050^\circ$ and $1,120^\circ\text{C}$ (App. 2, Table A7), and based on the Cr-Al orthopyroxene-spinel geothermometer (Voigt and von der Handt, 2011), chromite and orthopyroxene from the LG1 to MG1 layers equilibrated between $\sim 930^\circ$ and $1,170^\circ\text{C}$ (App. 2, Table A7). Thus, disseminated chromite could have reequilibrated with a liquid that was crystallizing plagioclase. However, it should be mentioned that the current study was not set up to carry out detailed temperature determinations, and thus these temperatures should be regarded as approximations. Further study would be required to refine the results.

The higher Fe# for disseminated chromite could in part be due to reequilibration with a fractionated liquid, as crystallization of chromite plus orthopyroxene would reduce the MgO concentrations in the liquid. In addition, it is well known that there is an Fe-Mg exchange between chromite and mafic minerals down to subsolidus temperatures (Roeder and Campbell, 1985; Scowen et al., 1991; Barnes, 1998). The increase in Fe# could be the result of Fe-Mg exchange with orthopyroxene in most layers, and with olivine in the LG4 layer. Based on the olivine-spinel Fe-Mg geothermometer (Ballhaus et al., 1991) the LG4 layer equilibrated between $\sim 800^\circ$ and 860°C . The equilibration temperature for all layers including the Merensky reef, for Fe-Mg exchange using the orthopyroxene-spinel geothermometer (Sato et al., 2008), covers a larger range (520° – 870°C ; App. 2, Table A7).

If the disseminated and chromitite chromite equilibrated at approximately the same temperatures, as indicated by the geothermometry, then why are the Cr# and Fe# different? The proportion of silicate minerals to chromite affects the concentrations of the elements in both the chromite and the mafic minerals. The Cr# and Fe# of the disseminated chromite must be much higher than that of the corresponding chromitite chromite in order that the equilibrium constants for Cr-Al and Fe-Mg exchange between chromite and orthopyroxene, or olivine remain the same. Thus, the disseminated chromites are displaced to higher Cr# and Fe# than chromitite chromites (Fig. 9B), despite the fact that they have equilibrated at approximately the same temperature.

The median ratios of (disseminated chromite)/(chromitite chromite) for Cr, Ga, and Ni and $\text{Fe}^{3+}/\text{Fe}_T$ are close to 1 (0.96–1.05; Fig. 11A) indicating very little change in Cr, Ga, and Ni contents and f_{O_2} . In contrast Fe_T , Mn, Co, and Zn show significant enrichments with ratios of 1.2 to 1.3 (Fig. 11A). Zinc shows a wider range of values than the other elements. As mentioned above, the increase in Fe_T in disseminated chromite is attributed to the combined effect of high silicate to chromite ratio and the Fe-Mg exchange with orthopyroxene. It is possible that the increases in Mn, Co, and Zn are also due to exchange with orthopyroxene, in which case the orthopyroxene from chromitite samples should contain less Mn, Co, and Zn than the orthopyroxene from samples with disseminated chromite. It is true that orthopyroxene from chromitite layers contains lower concentrations of these elements than some of the orthopyroxene from rocks with disseminated chromite (Fig. 15C, D). The exact level of enrichment may depend on the ratio of silicate to chromite and on the degree of fractionation of the liquid, and this is beyond the scope of the current work.

Relative to the chromite from adjacent chromitite layers, disseminated chromites are enriched in both Ti and V by a median factor of ~ 1.1 (Fig. 11A). We do not think that Ti and V diffused into chromite from orthopyroxene, because Ti is a 4+ ion and V is in the 3+, 4+, or 5+ state, and with such high charges neither element would be expected to readily diffuse at subsolidus temperatures. In addition, the concentrations of these elements in orthopyroxene are low (Fig. 15A, B), and it is therefore not a suitable source of Ti and V. We assume that the Ti and V enrichment is the result of reequilibration with the fractionated liquid.

The disseminated chromites are depleted in some elements (Hf, Zr, Cu, Sc, Mg, Al) relative to the chromitite chromites, from a low of 0.34 for Hf to a high of 0.8 for Al (Fig. 11A). As argued above, in the case of Al this is probably because the chromite reequilibrated with a fractionated liquid that had plagioclase on the liquidus. Similarly, chromite could be depleted in Sc due to competition for Sc from orthopyroxene. To explain the Hf and Zr depletion, we suggest that the fractionated liquid has reached zircon saturation, and for Cu a small amount of sulfide liquid may have segregated.

Effects of crystallization

Drage and Brenan (2023) carried out experiments over the temperature range $1,200^\circ$ to $1,280^\circ\text{C}$ and f_{O_2} at $\sim \Delta 0$ FMQ (where FMQ = fayalite-magnetite-quartz buffer) using the average B1 magma composition to investigate the composition of the chromite that could crystallize from this magma. Their resultant Cr# are similar to the compositions of the chromites from the chromitite layers (Fig. 9B, C). In addition, orthopyroxene is the mafic mineral that crystallized with the chromite, and the Mg# of the orthopyroxene from the experiments is similar to those reported from the Critical zone (Teigler and Eales, 1993; Godel et al., 2011; Eales and Costin, 2012; Cawthorn, 2015), indicating that the experiments successfully simulated the crystallization of the Critical zone.

However, these experiments did not produce a wide pressure and temperature interval with only chromite on the liquidus. In order to increase the interval with chromite only on the liquidus, some authors suggest that the proportion of

chromite that crystallized was increased by the addition of H₂O to the B1 magma (Mathez and Mey, 2005; Mathez and Kinzler, 2017). Veksler and Hou (2020) carried out experimental work to test this, using the B1 composition, starting with $f_{O_2} \Delta +1$ FMQ and no water. At 1,300°C this crystallized chromite as the sole liquidus phase and with Cr# in the range of Critical zone chromites, but with lower Fe# (Fig. 9B, C). The high $f_{O_2} \Delta +1$ FMQ, (which is higher than determined for the Bushveld chromite) resulted in both more Cr and more Fe in the 3+ state. The saturation of a melt in chromite is strongly dependent on f_{O_2} , and thus only chromite is on the liquidus in these experiments. The addition of 2, 4, and 6% water increased the f_{O_2} still further, which led to an increase in the Cr# and produced chromites that are more Fe rich than the chromites of the Bushveld. Furthermore, the addition of water suppressed orthopyroxene crystallization in favor of olivine. Thus, the addition of 2% water does not appear to mimic the conditions under which the Bushveld chromite crystallized. Nonetheless, as the magma crystallized, the H₂O content of the fractionated silicate melt would have increased, resulting in the crystallization of hydrous minerals such as phlogopite, but it is not clear that this would have any effect on chromite compositions.

The Cr# from chromite from the LG, MG, and UG2 chromitite layers match the Cr# from the Drage and Brenan (2023) experiments (Fig. 9B, C). It should be noted that the Cr# is highest in chromite from the LG4 layer and that the Cr₂O₃ content of chromite increases from the LG1 to LG4 but decreases up-section from the LG4 to UG2, implying that the LG4 chromite crystallized from the least fractionated liquid. The implied reversal in magma composition from LG1 to LG4 is also shown in the reversal in Mg# of the orthopyroxene in the silicate rocks (Teigler and Eales, 1993).

The chromite from UG1 and some chromites from the UG2 chromitite layers have slightly lower Cr# than those found in the Drage and Brenan experiments (Fig. 9C). It is possible that the UG1 and UG2 chromite with lower Cr# crystallized at a temperature lower than 1,200°C and that the Cr content of the liquid was lower than the 1,200°C experiments, as more orthopyroxene would have crystallized and thus the Cr content of the liquid would have been lower. In addition, if plagioclase was not yet on the liquidus then the Al content of the liquid would be higher, and the combined effect would lead to a lower Cr#.

Alternatively, another magma was present. Based on the presence of cumulate plagioclase and a sharp increase in initial ⁸⁷Sr/⁸⁶Sr values, many workers suggest that a second magma, known as the B2, was present at the level of the MG2 (Harmer and Sharpe, 1985; Kruger, 1994). However, the Cr content of the B2 magma is low and the oxide present is magnetite, not chromite (Harmer and Sharpe, 1985; Barnes et al., 2010), which suggests that the B2 magma was not responsible for the crystallization of chromite. To further test whether chromite could have crystallized from the B2 melt, the composition of spinel in equilibrium with the B2 was calculated using SPINMELTS2 (Nikolaev et al., 2018), and it is not chromite. SPINMELTS2 was used rather than MELTS because SPINMELTS2 calculates chromite compositions that closely approximate the results of the Drage and Brenan (2023) experiments. In contrast,

the compositions calculated by MELTS do not match the experimental results.

Although the B2 melt will not crystallize chromite, it is possible that the B2 magma was present in the magma chamber from the MG2 upward and that injections of B1 mixed with this magma. Simulations of the chromite composition based on a 50:50 mixture of B1 and B2 magma using SPINMELTS2 are similar to the UG1 chromite (Fig. 9C).

In contrast to Cr#, the Fe# of the chromitite chromite does not match the Fe# of the chromite from the experiments. The chromitite chromites are slightly more Fe rich than the chromites from the experiments (Fig. 9B, C). As outlined above, the high Fe# could be the result of Fe-Mg exchange with orthopyroxene in most layers and with olivine in the LG4 layer. The difference between the Fe# of chromite from the experiments and the chromitite chromite is much smaller than that of disseminated chromite because the proportion of chromite to orthopyroxene is much higher, as explained above. By the same token, as noted by Veksler et al. (2018) and Tang et al. (2023), the Mg# of orthopyroxene from the LG6, UG2, and UG3 chromitite tends to be higher than in the silicate rocks. This also appears to be the case in the current study, where the Mg# of orthopyroxenes from chromitites of the LG1 to LG6 are 0.86 to 0.91 (App. 2, Table A6), whereas Teigler and Eales (1993) report that the Mg# of the orthopyroxene from the associated silicate layers ranges from 0.82 to 0.88.

The minor and trace element contents of chromite can be compared with model contents for the initial chromite composition by multiplying the estimated element content of the liquid by the partition coefficient into chromite. For the LG to MG1 chromites, the liquid was assumed to be a fractionating B1 magma, assuming cotectic crystallization of the orthopyroxene and chromite and allowing for 18% fractionation between LG4 and LG1 and 25% between LG4 and MG1, based on the difference in Mg# of the orthopyroxenes in silicate rocks across the stratigraphy (Teigler and Eales, 1993). For the MG2 to UG2 section, the liquid was allowed to evolve by a further 15% fractionation. More details of the modeling are provided in Appendix 2, Table A8. As mentioned above it is possible that some B2 liquid was present, but as the concentrations of most of the elements being considered here are similar in the fractionated B1 and unfractionated B2, this would not greatly affect the composition of the liquid.

Gallium concentrations do not show a large difference between disseminated and chromitite chromite, and, after Cr, Ga is possibly the element closest to the original concentrations (Figs. 11A, 13A). Paktunc and Cabri (1995) report Ga concentrations in chromite from the UG2 chromitite of ~70 ppm, similar to the levels observed in our study. To model the composition of the chromite, they used a partition coefficient of 4.6 as determined by Malvin and Drake (1987). However, this partition coefficient is for Al spinel and slightly too high. In order to model the variations in Ga contents over the full stratigraphic section, we used a partition coefficient of 2.5 based on experiments for chromite Brenan et al. (2022).

The V content of the chromitite chromite from LG1 to LG5 can be broadly modeled with a partition coefficient of 10 (Fig. 11B). The LG6 chromite requires a higher partition coefficient of 15. For the MG1 to Merensky chromite interval a partition coefficient of 13 is required. The variation in partition

coefficient could be the result of changes in f_{O_2} . Vanadium can be in the 3+, 4+, or 5+ state, and V^{3+} partitions more readily into chromite than the V^{4+} or V^{5+} . The f_{O_2} can be calculated from the following equation (Nicklas et al., 2016):

$$\Delta \text{NNO} = (D^{\text{chr/liq}} - 6.1143) / -5.44, \quad (1)$$

which indicates an f_{O_2} of $\Delta \sim 0$ FMQ for the LG1 to LG5, an f_{O_2} of $\Delta -0.58$ FMQ for the MG2 to Merensky reef and $\Delta -0.93$ FMQ for LG6. These values lie within the range of f_{O_2} that can be estimated based on $\text{Fe}^{3+}/\text{Fe}_T$ ratios (Ballhaus et al., 1991), which range from 0.2 to 0.3 (Fig. 10E) and which imply a range in f_{O_2} of $\sim \Delta -1$ to 0 FMQ for the crystallization of the chromite.

The bulk partition coefficients of Mn, Co, Zn, and Ni for crystallization of orthopyroxene and chromite in cotectic proportions would all be around 1. Because the concentrations of the elements in the liquid have not changed appreciably, the modeled concentrations of these elements in chromite remain relatively constant across the section. Lines showing modeled composition for the chromite are similar to the chromitite chromite compositions for Mn, Co, and Ni for all layers, (Fig. 12C-E). An exception to this is that Ni concentrations are somewhat higher in the UG2 chromite and much higher in the Merensky reef chromite. This point was also noted by Ning et al. (2024), who attributed it to the presence of sulfides in these layers. In fact, despite being rich in PGEs, the UG2 and Merensky chromite layers in our samples contain very little sulfide (Barnes and Maier, 2002; Maier and Barnes, 2008), and this is also the case at other localities. The low sulfide content of the chromite layers has been attributed to S loss from these layers during reequilibration with chromite (Naldrett and Lehmann, 1988; Barnes and Maier, 2002) and/or dissolution of the sulfides by late magmatic liquid. If a liquid dissolved the sulfide, then possibly Ni was released and could have diffused into the chromite. Zinc shows a sudden increase at the LG4 level and persists at higher concentrations from this point onward (Fig. 12F). The reason for this is not understood.

The bulk D for Sc would also have been ~ 1 , and the chromitite chromite should have a relatively uniform composition as the concentration in the liquid should not have varied much. Assuming an Sc concentration in the magma of 30 ppm (both B1 and B2 magmas contain Sc at this concentration) and a partition coefficient of 0.2 between chromite and liquid, the chromite should contain ~ 6 ppm Sc. The chromitite chromite concentrations are of this order of magnitude (4–10 ppm) but variable. This could reflect analytical variations or true variation in the chromite concentrations. Analytical error as defined by two standard deviations on individual grains is ~ 0.2 ppm, thus the variation is not attributable to analytical error. BC-16, our in-house chromite reference material from the UG2 chromitite layer from Western Platinum mine, was analyzed in every run for a total of 18 times with an average of 7.5 ppm with a standard deviation of ± 1.5 ppm. Therefore, most of the variation in BC-16 appears to be due to heterogeneity from grain to grain. The variation may in part be due to reequilibration with orthopyroxene. In this case one would expect the Sc concentrations of orthopyroxene in chromitite layers to be higher than those of the orthopyroxene in rocks with disseminated chromite, and this is indeed the case for some of the orthopyroxenes (Fig. 14A). When we allow for

two standard deviations, the range of values in BC-16 covers the range of values observed for all the chromite.

Hafnium is incompatible with chromite, orthopyroxene, and plagioclase; therefore, the concentrations of Hf in the chromitite should increase as the liquid evolves. The B1 and B2 liquids have similar Hf concentrations, and so the possible addition of B2 magma does not change the modeled concentrations by much. Overall Hf concentrations in chromite from the LG chromitite layers to the UG2 chromitite layers increase as predicted; however, it should be understood that at these low concentration levels large errors are possible (Fig. 13E).

The Ti contents of the chromite from the LG chromitite layers are on average 1.5 times higher than those found in the chromite of the experiments of Drage and Brenan (2023) and Veksler and Hou (2020). Modeling using published partition coefficients of 0.7 gives results similar to the experiments (Fig. 12A). Either the assumed Ti contents of the magma are too low or the partition coefficient of Ti between chromite and melt is strongly dependent on temperature and composition. It is possible that the Ti concentrations for the liquid based on the Bushveld sills are too low; however, estimates of the Ti content of the liquid of the Lower Critical zone based on the silicate rocks indicate that the Ti content of the liquid was similar to the B1 magma (Godel et al., 2011). For the chromites from the Upper Critical zone, assuming a 50% B1 and B2 magma mixture, the model Ti content of the chromite is slightly higher (3,100 ppm) but not sufficient to match the observed Ti content of the chromite (Fig. 12A). The partitioning of Ti into chromite is a coupled substitution of Fe^{2+} and Ti^{4+} into the octahedral site and is dependent on the magnetite component of the spinel. Given that the chromite is richer in FeO than the FeO determined by experiments, we suggest that the high Ti is the combined effect of an increase in partition coefficient due to change in spinel composition and decrease in temperature.

Model for composition of chromite

There are a number of models for the formation of the chromitite layers. The classic model is that magma became saturated in only chromite on the liquidus because of a sudden change in one of the intensive variables: an increase in f_{O_2} (Ulmer, 1969; Murck and Campbell, 1986; Roeder and Reynolds, 1991); a change in pressure (Lipin, 1992; Cawthorn, 2005; Latypov et al., 2022); a change in composition brought about by magma mixing or contamination with crustal melts (Irvine, 1977; Kinnaird et al., 2002; Spandler et al., 2005); or conversion of banded Fe stone to chromitite (Leshner et al., 2019). Alternatively, models considering physical accumulation of chromite have been proposed (Mondal and Mathez, 2007; Maier et al., 2013; Forien et al., 2015; Mukherjee et al., 2017; Roelofse et al., 2024). Finally, reaction between orthopyroxene and late magmatic fluids has been considered (Marsh et al., 2021; Boudreau, 2025). Further complicating any model for the formation of chromitite layers is the question of whether the layers were emplaced strictly in sequence or were out of sequence and how much melt was present in the magma chamber at any one time. Based on U-Pb zircon and baddeleyite age dating, Mungall et al. (2016) and Scoates et al. (2021) have argued that the chromitite layers were not emplaced in sequence, with the UG chromitites being older

than the underlying MG chromitites. However, the concept of out-of-sequence emplacement is strongly contested (Latypov et al., 2017). Space constraints make it impossible to address each of these models, and therefore in the discussion below we focus the evolution of the composition of the chromite.

In most chromitite layers, chromite is in equilibrium with the B1 melt or a fractionated product of the B1 that had both chromite and orthopyroxene on the liquidus. Aluminum, V, Cr, Mn, Fe, Co, Ni, Zn, and Ga partitioned into the chromite. This chromite accumulated on the cumulate pile (Fig. 17A), with the average chromitite containing ~80 wt % chromite (~73 modal % chromite). The silicate component consists of a mixture of liquid fraction and silicate cumulate fraction. Based on the incompatible element concentrations (Hf, La, and Sm) and assuming the trapped liquid was similar to initial B1, the trapped liquid fraction can be determined to be on average ~8 wt % (App. 2, Table A5). In fact, it could be even lower, as the fractionated liquid would have had higher incompatible element contents than the initial liquid. The balance of the silicate fraction made up of the oikocrysts must be thought of as ce-

ment, which as they crystallized displaced liquid and enclosed some small grains of chromite (Fig. 17B). At the same time, textural maturation resulted in some small chromite grains being dissolved and reprecipitated onto larger grains (Fig. 17B).

Some small chromite grains could have settled into fractionated liquid of the underlying cumulate mush (Fig. 17C). The chromite would not have been in equilibrium with this liquid and would have reequilibrated with it. The fractionated liquid would have been depleted in Sc, Mg, and Al because of the crystallization of orthopyroxene and plagioclase, and the chromite could have lost these elements to the liquid, resulting in high Cr# and Sc depletion for the disseminated chromite. At lower temperatures zircon and sulfide liquid were on the liquidus, resulting in lower Zr, Hf, and Cu concentrations in the disseminated chromite.

The higher Mn, Co, and Zn contents of disseminated chromite than chromitite chromite could in part be due to reequilibration with fractionated liquid. However, the Fe-Mg exchange between chromite and orthopyroxene on average occurred down to subsolidus temperatures (~500°–700°C),

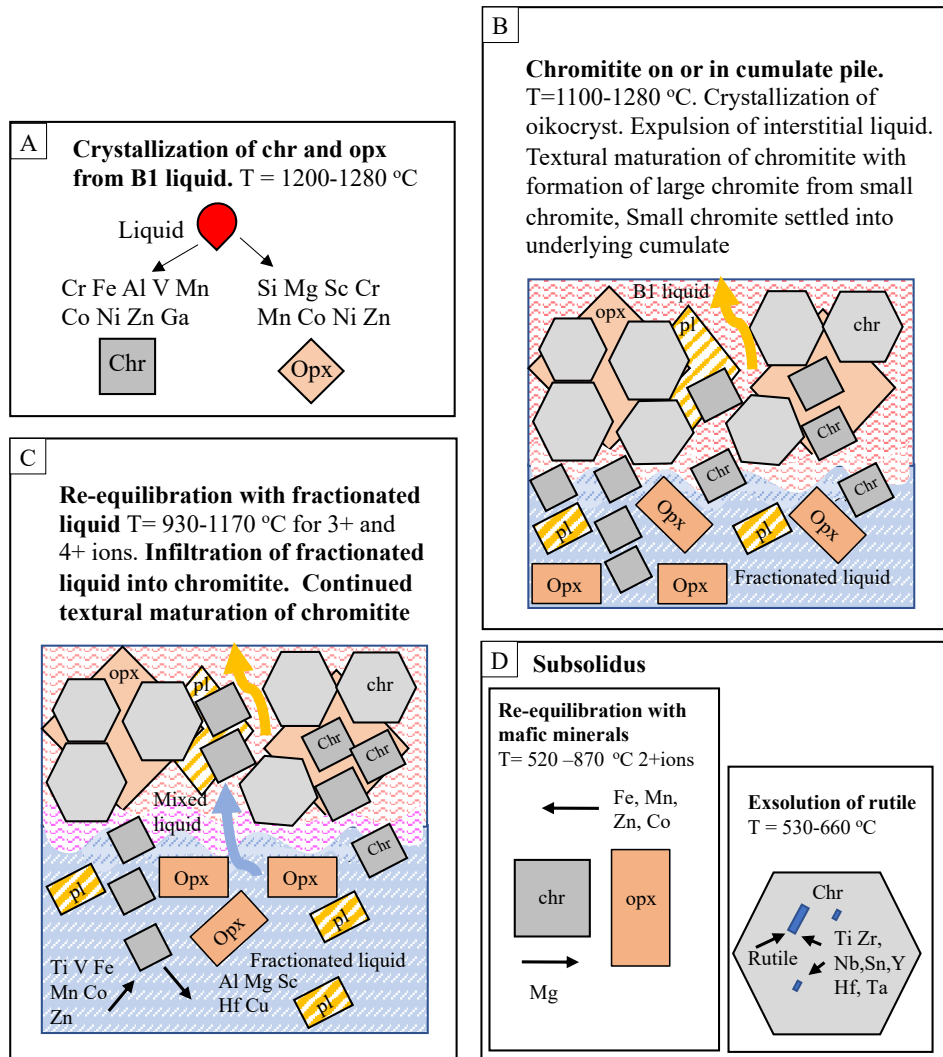


Fig. 17. Model of changes in element concentrations with development of chromite layers. Abbreviations: chr = chromite, opx = orthopyroxene, pl = plagioclase.

and presumably these elements could also have reequilibrated during this process (Fig. 17D). Another process that occurred subsolidus is the exsolution of rutile from chromite, with an enrichment of Ti, Zr, Nb, Sn, Y, Hf, and Ta in the rutile grains (Fig. 17D). Based on the Ferry and Watson (2007) Zr-in-rutile thermometer, the rutile exsolution in our chromites formed between 540° and 660°C (App. 2, Table A7), which is agreement with the more detailed study by Ver Hoeve et al. (2018).

There are number of thin layers (<2.5 cm) of chromite in the Critical zone that we did not sample. As pointed out by Scoon and Costin (2018), the thin layers do not necessarily have the same origin as the thick chromite layers. However, given the economic importance of the Merensky reef, the chromite from the upper and lower thin chromite layers in the Merensky reef were analyzed. Recent work describing various models for the formation of Merensky reef are fairly complex (Scoon and Costin, 2018; Hayes et al., 2025; Smith et al., 2025) and will not be dealt with here. The purpose of the discussion below is simply to compare chromite compositions from the reef with the composition of chromite from the chromitite layers. On the Cr# versus Fe# plot, the Merensky amoeboidal chromites from the lower chromite layer plot on the upper edge of the UG1 and UG2 chromitite chromite fields (Fig. 9C). The small euhedral chadacryst chromites just above the lower seam plot along the trend for reequilibration with higher Cr# and Fe# (Fig. 9C). The Cr# and Fe# of the Merensky chromite from the upper chromite layer plot further along the reequilibration vector. They are similar in composition to the matrix chromite of the UG2 (Fig. 9C). The most extreme composition is that of the disseminated chromite from between the two layers (Fig. 9C). This is also the case for most the minor and trace element concentrations (Figs. 10, 12, 13). The composition of the chromite from the Merensky chromite layers suggests the chromite could have originally been in equilibrium with a magma similar to the UG2 magma, but subsequently the chromite has reacted with a fractionated liquid.

Conclusions

The Cr# of the chromitite layers from the LG1 to the MG4 is similar to those obtained from experiments simulating the crystallization of the initial Bushveld magma (B1) over the temperature interval 1,200° to 1,280°C at $f_{O_2} \sim \Delta 0$ FMQ. The Cr# of some UG1 and UG2 chromites are slightly lower, possibly because of equilibration at lower temperature or mixing of incoming B1 magma with a resident B2 magma. The minor and trace element contents of most chromite from chromitite layers can also be modeled by crystallization from a fractionating B1 liquid. However, Ti concentrations in chromite are higher than results from experiments. Chromitite layers contain on average 20 wt % silicate component. Less than half of this represents trapped liquid component, with the balance representing cement, now in the form of oikocrysts.

Fe# of the chromite from chromitite is slightly higher than that obtained in experiments. The estimated temperature of equilibration between chromite and orthopyroxene based on Fe-Mg exchange indicates that chromite and orthopyroxene reequilibrated to fairly low temperatures (520°–879°C), and the higher Fe# in the Bushveld chromite relative to the experiments is attributed to this. Possibly, along with the increase in Fe in the chromite, Ti concentrations also increased.

Comparison of the composition of chromite from silicate rocks with chromite from the adjacent chromitite layers shows that silicate-hosted chromite contains higher concentrations of Fe, Ti, V, Mn, Co, and Zn and lower concentrations of Mg, Al, Sc, Cu, and Hf than the chromitite chromite. These differences can be attributed to the combined effects of reequilibration with a fractionated liquid and the higher silicate to chromite ratios in the orthopyroxenites and norites compared to chromitite. Accompanying these changes in chromite composition are complementary changes in orthopyroxene, which is the other major mineral present. Orthopyroxene in the chromitite is richer in Mg and Sc than orthopyroxene from orthopyroxenites or norites. Chrome, Ga, Ni concentrations and Fe^{3+}/Fe_T ratios are similar in both types of chromite.

Small rutile exsolutions formed between 500° and 700°C and these are enriched in Ti, Zr, Nb, Hf, and Ta.

Acknowledgments

We would like to thank Marc Constantin and Audrey Lavoie for their excellent assistance with the microprobe and laser ablation analyses. Rais Latypov, Louis Cabri, and the editor are thanked for their time and efforts to improve the manuscript. This work was supported by a Natural Science and Engineering Discovery grant (1884-2013) to SJB.

Competing Interests

The authors declare there are no competing interests.

Roles of the Authors

1. Sarah-Jane Barnes: Data collection, composition of the manuscript, drafting figures;
2. Wolfgang Maier: Sample collection, geologic setting information, discussion, editing;
3. Dany Savard: Treatment of laser ablation data;
4. Steve A. Prevec: Sample collection, geologic setting information, discussion, editing.

REFERENCES

- Arunachellan, Y., 2022, Constraints on Cr-PGE mineralisation: Geochemistry and petrology of the Middle Group 1 and 3 chromitites, Western limb, Bushveld Complex, South Africa: M.Sc. thesis, Makhanda, South Africa, Rhodes University, 123 p.
- Bai, Y., Su, B.-X., Xiao, Y., Cui, M.-M., and Charlier, B., 2021, Magnesium and iron isotopic evidence of inter-mineral diffusion in ultramafic cumulates of the Peridotite zone, Stillwater Complex: *Geochimica et Cosmochimica Acta*, v. 292, p. 152–169.
- Ballhaus, C., Berry, R.F., and Green, D.H., 1991, High pressure experimental calibration of the olivine-orthopyroxene-spinel oxygen geobarometer: Implications for the oxidation state of the upper mantle: *Contributions to Mineralogy and Petrology*, v. 107, p. 27–40, <https://doi.org/10.1007/BF00311183>.
- Barnes, S.J., 1986, The distribution of chromium among orthopyroxene, spinel and silicate liquid at atmospheric pressure: *Geochimica et Cosmochimica Acta*, v. 50, p. 1889–1909.
- 1998, Chromite in komatiites, 1. Magmatic controls on crystallization and composition: *Journal of Petrology*, v. 39, p. 1689–1720.
- Barnes, S.J., and Roeder, P.L., 2001, The range of spinel compositions in terrestrial mafic and ultramafic rocks: *Journal of Petrology*, v. 42, p. 2279–2302.
- Barnes, S.-J., 2024, Platinum-group element and trace element contents of chromite grains from the Alexo komatiite flows compared with chromites from other volcanic rocks: Implications for the use of chromite compositions in petrogenesis: *The Canadian Journal of Mineralogy and Petrology*, v. 62, p. 659–681.

- Barnes, S.-J., and Maier, W.D., 2002, Platinum-group elements and microstructures of normal Merensky reef from Impala platinum mines, Bushveld Complex: *Journal of Petrology*, v. 43, p. 103–128.
- Barnes, S.-J., Maier, W.D., and Curl, E.A., 2010, Composition of the marginal rocks and sills of the Rustenburg Layered Suite, Bushveld Complex, South Africa: Implications for the Formation of the platinum-group element deposits: *Economic Geology*, v. 105, p. 1491–1511.
- Barnes, S.-J., Mansur, E.T., Maier, W.D., and Prevec, S.A., 2023, A comparison of trace element concentrations in chromite from komatiites, picrites, and layered intrusions: Implications for the formation of massive chromite layers: *Canadian Journal of Earth Sciences*, v. 60, p. 97–132.
- Bates, R.L., and Jackson, J.A., 1987, *Glossary of geology*: Alexandria, American Geological Institute, 788 p.
- Boudreau, A.E., 2025, Formation of PGE- and sulfide-bearing chromitites and associated anorthositic rocks in layered intrusions by the infiltration of reactive, Cl-rich fluid: *Geological Society, London, Special Publications*, v. 552, <https://doi.org/10.1144/SP552-2022-324>.
- Brenan, J.M., Woods, K., Mungall, J.E., and Weston, R., 2022, Origin of chromitites in the Esker intrusion complex, Ring of Fire intrusive suite, as revealed by chromite trace element chemistry and simple crystallization models: *Geological Survey of Canada, Open File 8755*, p. 1–19.
- Cawthorn, R.G., 2005, Pressure fluctuations and the formation of the PGE-rich Merensky and chromitite reefs, Bushveld Complex: *Mineralium Deposita*, v. 40, p. 231–235.
- 2015, The Bushveld Complex, South Africa, in Charlier, B., Namur, O., Latypov, R., and Tegner, C., eds., *Layered intrusions*: Dordrecht, Springer Netherlands, p. 517–587.
- Coogan, L., Saunders, A., and Wilson, R., 2014, Aluminum-in-olivine thermometry of primitive basalts: Evidence of an anomalously hot mantle source for large igneous provinces: *Chemical Geology*, v. 368, p. 1–10.
- Coulthard, D.A., Zellmer, G.F., Tomiya, A., Jégo, S., and Brahm, R., 2021, Petrogenetic implications of chromite-seeded boninite crystallization experiments: Providing a basis for chromite-melt diffusion chronometry in an oxybarometric context: *Geochimica et Cosmochimica Acta*, v. 297, p. 179–202.
- Cousins, C., and Feringa, G., 1964, The chromite deposits of the western belt of the Bushveld Complex, in Houghton, S.H., ed., *The geology of some ore deposits in Southern Africa*: Johannesburg, Geological Society of South Africa, p. 183–202.
- Drage, N., and Brenan, J., 2023, An experimental study of the effect of pressure on the formation of chromite deposits: *Journal of Petrology*, v. 64, p. 1–26.
- Eales, H.V., and Costin, G., 2012, Crustally contaminated komatiite: Primary source of the chromitites and Marginal, Lower, and Critical zone magmas in a staging chamber beneath the Bushveld Complex: *Economic Geology*, v. 107, p. 645–665.
- Eales, H.V., and Reynolds, I.M., 1986, Cryptic variations within chromitites of the Upper Critical zone, northwestern Bushveld Complex: *Economic Geology*, v. 81, p. 1056–1066.
- Ferry, J., and Watson, E., 2007, New thermodynamic models and revised calibrations for the Ti-in-zircon and Zr-in-rutile thermometers: *Contributions to Mineralogy and Petrology*, v. 154, p. 429–437.
- Forien, M., Tremblay, J., Barnes, S.-J., Burgisser, A., and Page, P., 2015, The role of viscous particle segregation in forming chromite layers from slumped crystal slurries: Insights from analogue experiments: *Journal of Petrology*, v. 56, p. 2425–2444.
- Ghiorso, M.S., and Gualda, G.A., 2015, An H₂O-CO₂ mixed fluid saturation model compatible with rhyolite-MELTS: *Contributions to Mineralogy and Petrology*, v. 169, p. 1–30.
- Godel, B., Barnes, S.-J., and Maier, W. D., 2011, Parental magma composition inferred from trace element in cumulus and intercumulus silicate minerals: An example from the Lower and Lower Critical zones of the Bushveld Complex, South-Africa: *Lithos*, v. 125, p. 537–552.
- Harmer, R.E., and Sharpe, M.R., 1985, Field relations and strontium isotope systematics of the eastern Bushveld Complex: *Economic Geology*, v. 80, p. 813–837.
- Hayes, B., Maghdour-Mashhour, R., Ashwal, L.D., Smith, A.J., Uecker-mann, H., and Vermeulen, J., 2025, Melt infiltration in a crystal mush and pegmatoid formation in the platinumiferous Merensky reef, Bushveld Complex, South Africa: *Mineralium Deposita*, v. 60, p. 237–259, <https://doi.org/10.1007/s00126-024-01278-z>.
- Hill, R., and Roeder, P., 1974, The crystallization of spinel from basaltic liquid as a function of oxygen fugacity: *The Journal of Geology*, v. 82, p. 709–729.
- Holness, M.B., Vukmanovic, Z., and O'Driscoll, B., 2023, The formation of chromite chains and clusters in igneous rocks: *Journal of Petrology*, v. 64, p. 1–24.
- Hunt, E.J., O'Driscoll, B., and Day, J.M., 2021, Sintering as a key process in the textural evolution of chromitite seams in layered mafic-ultramafic intrusions: *The Canadian Mineralogist*, v. 59, p. 1661–1692.
- Irvine, T.N., 1977, Origin of chromitite layers in Muskox Intrusion and other stratiform intrusions—new interpretation: *Geology*, v. 5, p. 273–277.
- Junge, M., Oberthür, T., and Melcher, F., 2014, Cryptic variation of chromite chemistry, platinum group element and platinum group mineral distribution in the UG-2 chromitite: An example from the Karee mine, western Bushveld Complex, South Africa: *Economic Geology*, v. 109, p. 795–810.
- Junge, M., Oberthür, T., Osbahr, I., and Gutter, P., 2016, Platinum-group elements and minerals in the lower and middle group chromitites of the western Bushveld Complex, South Africa: *Mineralium Deposita*, v. 51, p. 841–852.
- Kamenetsky, V.S., Crawford, A.J., and Meffre, S., 2001, Factors controlling chemistry of magmatic spinel: An empirical study of associated olivine, Cr-spinel and melt inclusions from primitive rocks: *Journal of Petrology*, v. 42, p. 655–671.
- Kaufmann, F.E.D., Hoffmann, M.C., Bachmann, K., Veksler, I.V., Trumbull, R.B., and Hecht, L., 2019, Variations in composition, texture, and platinum group element mineralization in the Lower Group and Middle Group chromitites of the northwestern Bushveld Complex, South Africa: *Economic Geology*, v. 114, p. 569–590.
- Kinnaird, J.A., Kruger, F.J., Nex, P.A.M., and Cawthorn, R.G., 2002, Chromitite formation—a key to understanding processes of platinum enrichment: *Applied Earth Science*, v. 111, p. 23–35.
- Kruger, F.J., 1994, The Sr-isotopic stratigraphy of the western Bushveld Complex: *South African Journal of Geology*, v. 97, p. 393–398.
- Langa, M.M., Jugo, P.J., Leybourne, M.I., Grobler, D.F., Adetunji, J., and Skogby, H., 2021, Chromite chemistry of a massive chromitite seam in the northern limb of the Bushveld Igneous Complex, South Africa: Correlation with the UG-2 in the eastern and western limbs and evidence of variable assimilation of footwall rocks: *Mineralium Deposita*, v. 56, p. 31–44.
- Latypov, R., Chistyakova, S., and Mukherjee, R., 2017, A novel hypothesis for origin of massive chromitites in the Bushveld Igneous Complex: *Journal of Petrology*, v. 58, p. 1899–1940.
- Latypov, R., Chistyakova, S., Barnes, S.J., et al., 2022, Chromitite layers indicate the existence of large, long-lived, and entirely molten magma chambers: *Scientific Reports*, v. 12, article 4092.
- Latypov, R., Chistyakova, S.Y., and Letsoele, C., 2024, Massive chromitites of the Bushveld Complex, South Africa: A critical review of existing hypotheses: *Earth-Science Reviews*, v. 256, article 104858, <https://doi.org/10.1016/j.earscirev.2024.104858>.
- Lenaz, D., Garuti, G., Zaccarini, F., Cooper, R., and Princivalle, F., 2012, The Stillwater Complex chromitites: The response of chromite crystal chemistry to magma injection: *Geologica Acta* v. 10, p. 1–10.
- Leshner, C., Carson, H., and Houlié, M., 2019, Genesis of chromite deposits by dynamic upgrading of Fe ± Ti oxide xenocrysts: *Geology*, v. 47, p. 207–210.
- Leuthold, J., Blundy, J.D., and Brooker, R.A., 2015, Experimental petrology constraints on the recycling of mafic cumulate: A focus on Cr-spinel from the Rum Eastern layered intrusion, Scotland: *Contributions to Mineralogy and Petrology*, v. 170, p. 1–27.
- Lipin, B.R., 1992, Pressure increases, the formation of chromite seams, and the development of the Ultramafic Series in the Stillwater Complex, Montana: *Journal of Petrology*, v. 34, p. 955–976.
- Maier, W., and Barnes, S.-J., 2008, Platinum-group elements in the UG1 and UG2 chromitites, and the Bastard reef, at Impala platinum mine, western Bushveld Complex, South Africa: Evidence for late magmatic cumulate instability and reef constitution: *South African Journal of Geology*, v. 111, p. 159–176.
- Maier, W.D., and Bowen, M.P., 1996, The UG2-Merensky reef interval of the Bushveld Complex northwest of Pretoria: *Mineralium Deposita*, v. 31, p. 386–393.
- Maier, W.D., and Eales, H.V., 1997, Correlation within the UG2-Merensky reef interval of the Western Bushveld Complex, based on geochemical, mineralogical, and petrological data: *Geological Survey of South Africa Bulletin*, v. 120, 56 p.
- Maier, W.D., Prichard, H.M., Barnes, S.-J., and Fisher, P.C., 1999, Compositional variation of laurite at Union section in the western Bushveld Complex: *South African Journal of Geology*, v. 102, p. 286–292.

- Maier, W.D., Barnes, S.-J., and Groves, D., 2013, The Bushveld Complex, South Africa: Formation of platinum-palladium, chrome- and vanadium-rich layers via hydrodynamic sorting of a mobilized cumulate slurry in a large, relatively slowly cooling, subsiding magma chamber: *Mineralium Deposita*, v. 48, p. 1–56.
- Maier, W.D., Barnes, S.-J., Muir, D., Savard, D., Lahaye, Y., and Smith, W., 2021, Formation of Bushveld anorthosite by reactive porous flow: Contributions to Mineralogy and Petrology, v. 176, p. 1–12.
- Malvin, D.J., and Drake, M.J., 1987, Experimental determination of crystal/melt partitioning of Ga and Ge in the system forsterite-anorthite-diopside: *Geochimica et Cosmochimica Acta*, v. 51, p. 2117–2128.
- Mansur, E.T., and Barnes, S.-J., 2020, The role of Te, As, Bi, Sn and Sb during the formation of platinum-group-element reef deposits: Examples from the Bushveld and Stillwater Complexes: *Geochimica et Cosmochimica Acta*, v. 272, p. 235–258.
- Marsh, J.S., Pasecznyk, M.J., and Boudreau, A.E., 2021, Formation of chromitite seams and associated anorthosites in layered intrusion by reactive volatile-rich fluid infiltration: *Journal of Petrology*, v. 62, article egaa109.
- Mathez, E.A., and Kinzler, R.J., 2017, Metasomatic chromitite seams in the Bushveld and Rum layered intrusions: *Elements*, v. 13, p. 397–402.
- Mathez, E.A., and Mey, J.L., 2005, Character of the UG2 chromitite and host rocks and petrogenesis of its pegmatoidal footwall, northeastern Bushveld Complex: *Economic Geology*, v. 100, p. 1617–1630.
- Mondal, S.K., and Mathez, E.A., 2007, Origin of the UG2 chromitite layer, Bushveld Complex: *Journal of Petrology*, v. 48, p. 495–510.
- Mukherjee, R., Latypov, R., and Balakrishna, A., 2017, An intrusive origin of some UG-1 chromitite layers in the Bushveld Igneous Complex, South Africa: Insights from field relationships: *Ore Geology Reviews*, v. 90, p. 94–109.
- Mungall, J.E., Kamo, S.L., and McQuade, S., 2016, U-Pb geochronology documents out-of-sequence emplacement of ultramafic layers in the Bushveld Igneous Complex of South Africa: *Nature Communications*, v. 7, article 13385.
- Murck, B.W., and Campbell, I.H., 1986, The effects of temperature, oxygen fugacity and melt composition on the behaviour of chromium in basic and ultrabasic melts: *Geochimica et Cosmochimica Acta*, v. 50, p. 1871–1887.
- Naldrett, A.J., and Lehmann, J., 1988, Spinel non-stoichiometry as the explanation for Ni-, Cu- and PGE-enriched sulphides in chromitites, in Prichard, H.M., Potts, P.J., Bowles, J.F.W., and Cribb, S.J., eds., *Geo-platinum 87*: Dordrecht, Springer Netherlands, p. 93–109.
- Naldrett, A., Kinnaird, J., Wilson, A., Yudovskaya, M., McQuade, S., Chunnett, G., and Stanley, C., 2009, Chromite composition and PGE content of Bushveld chromitites: Part 1—the Lower and Middle Groups: *Applied Earth Science*, v. 118, p. 131–161.
- Naldrett, A., Wilson, A., Kinnaird, J., Yudovskaya, M., and Chunnett, G., 2012, The origin of chromitites and related PGE mineralization in the Bushveld Complex: New mineralogical and petrological constraints: *Mineralium Deposita*, v. 47, p. 209–232.
- Nicklas, R.W., Puchtel, I.S., and Ash, R.D., 2016, High-precision determination of the oxidation state of komatiite lavas using vanadium liquid-mineral partitioning: *Chemical Geology*, v. 433, p. 36–45.
- Nikolaev, G.S., Ariskin, A.A., and Barmina, G.S., 2018, SPINMELT-2.0: Simulation of spinel-melt equilibrium in basaltic systems under pressures up to 15 kbar: II. Description of the program package, the topology of the Cr-spinel-melt model system, and petrological implications: *Geochemistry International*, v. 56, p. 125–135.
- Ning, S., Su, B.-X., Tang, D.-M., Luo, Y., Yuan, Q.-H., and Bai, Y., 2024, Cobalt and nickel distribution and controlling factors in the Bushveld layered complex: *Ore Geology Reviews*, v. 170, article 106130, <https://doi.org/10.1016/j.oregeorev.2024.106130>.
- Oberthür, T., Junge, M., Rudashevsky, N., de Meyer, E., and Gutter, P., 2016, Platinum-group minerals in the LG and MG chromitites of the eastern Bushveld Complex, South Africa: *Mineralium Deposita*, v. 51, p. 71–87.
- Osbahr, I., Oberthür, T., Klemd, R., and Josties, A., 2014, Platinum-group element distribution in base-metal sulfides of the UG2 chromitite, Bushveld Complex, South Africa—a reconnaissance study: *Mineralium Deposita*, v. 49, p. 655–665.
- Pagé, P., and Barnes, S.-J., 2016, The influence of chromite on osmium, iridium, ruthenium and rhodium distribution during early magmatic processes: *Chemical Geology*, v. 420, p. 51–68.
- Paktunc, A.D., and Cabri, L.J., 1995, A proton- and electron-microprobe study of gallium, nickel and zinc distribution in chromian spinel: *Lithos*, v. 35, p. 261–282.
- Park, J.-W., Campbell, I.H., and Eggins, S.M., 2012, Enrichment of Rh, Ru, Ir and Os in Cr spinels from oxidized magmas: Evidence from the Ambae volcano, Vanuatu: *Geochimica Cosmochimica Acta*, v. 78, p. 28–50.
- Paton, C., Hellstrom, J., Paul, B., Woodhead, J., and Hergt, J., 2011, Iolite: Freeware for the visualisation and processing of mass spectrometric data: *Journal of Analytical Atomic Spectrometry*, v. 26, p. 2508–2518.
- Pebane, M., and Latypov, R., 2017, The significance of magmatic erosion for bifurcation of UG1 chromitite layers in the Bushveld Complex: *Ore Geology Reviews*, v. 90, p. 65–93.
- Prichard, H.M., Barnes, S.-J., Maier, W.D., and Fisher, P., 2004, Variation of PGM in a cross section through the Merensky reef at Impala mines: *Canadian Mineralogist*, v. 42, p. 423–437.
- Roeder, P.L., and Campbell, I.H., 1985, The effect of postcumulus reactions on composition of chrome-spinels from the Jimberlana intrusion: *Journal of Petrology*, v. 26, p. 763–786.
- Roeder, P.L., and Reynolds I., 1991, Crystallization of chromite and chromium solubility in basaltic melts: *Journal of Petrology*, v. 32, p. 909–934.
- Roelofse, F., Magson, J., Nicholson, M., and Nyakane, T., 2024, A high-resolution geochemical and petrological investigation of bifurcating chromitite layers of the UG1 footwall at Impala platinum mine, Rustenburg: *The Canadian Journal of Mineralogy and Petrology*, v. 62, p. 713–730.
- Sato, K., Miyamoto, T., and Kawasaki, T., 2008, Fe²⁺-Mg partitioning experiments between orthopyroxene and spinel using ultrahigh-temperature granulite from the Napier Complex, east Antarctica: *Geological Society, London, Special Publications*, v. 308, p. 431–447.
- Scoates, J.S., Wall, C.J., Friedman, R.M., Weis, D., Mathez, E.A., and Van-Tongeren, J.A., 2021, Dating the Bushveld Complex: Timing of crystallization, duration of magmatism, and cooling of the world's largest layered intrusion and related rocks: *Journal of Petrology*, v. 62, article egaa107.
- Scoon, R.N., and Costin, G., 2018, Chemistry, morphology and origin of magmatic-reaction chromite stringers associated with anorthosite in the Upper Critical zone at Winaarshoek, Eastern limb of the Bushveld Complex: *Journal of Petrology*, v. 59, p. 1551–1578.
- Scoon, R.N., and Teigler, B., 1994, Platinum-group element mineralization in the Critical zone of the western Bushveld Complex; I, Sulfide poor-chromitites below the UG-2: *Economic Geology*, v. 89, p. 1094–1121.
- Scowen, P.A.H., Roeder, P.L., and Helz, R.T., 1991, Re-equilibration of chromite within Kilauea Iki lava lake, Hawaii: *Contributions to Mineralogy and Petrology*, v. 107, p. 8–20.
- Smith, W.D., Henry, H., Heinonen, J.S., et al., 2025, Role of chamber replenishment in the formation of the Merensky reef and its footwall anorthosite: *Journal of Petrology*, v. 66, article egaf015, <https://doi.org/10.1093/petrology/egaf015>.
- South African Committee for Stratigraphy, 1980, Stratigraphy of southern Africa. Part 1. Lithostratigraphy of South Africa, South West Africa/Namibia, and the Republics of Bophuthatswana, Transkei, and Venda: *Geological Survey of South Africa, Handbook 8*, 690 p.
- Spandler, C., Mavrorogenes, J., and Arculus, R., 2005, Origin of chromitites in layered intrusions: Evidence from chromite-hosted melt inclusions from the Stillwater Complex: *Geology*, v. 33, p. 893–896.
- Suzuki, A., Yasuda, A., and Ozawa, K., 2008, Cr and Al diffusion in chromite spinel: Experimental determination and its implication for diffusion creep: *Physics and Chemistry of Minerals*, v. 35, p. 433–445.
- Tang, D., Qin, K., Evans, N.J., and Fang, L., 2023, Silicate mineral inclusions in chromite from the eastern Bushveld Complex: Implications for the origin and evolution of hydrous melt during chromite mineralization in the Critical zone: *Lithos*, v. 438, article 106997.
- Teigler, B., 1990, Platinum group element distribution in the Lower and Middle group chromitites in the Western Bushveld Complex: *Mineralogy and Petrology*, v. 42, p. 165–179.
- Teigler, B., and Eales, H., 1993, Correlation between chromite composition and PGE mineralization in the Critical zone of the western Bushveld Complex: *Mineralium Deposita*, v. 28, p. 291–302.
- Ulmer, G.C., 1969, Experimental investigations of chromite spinels: *Economic Geology Monograph 4*, p. 114–131.
- U.S. Geological Survey, 2021, Mineral commodity summaries 2021: 200 p., <https://doi.org/10.3133/mcs2021>.
- Vekslar, I.V., and Hou, T., 2020, Experimental study on the effects of H₂O upon crystallization in the Lower and Critical zones of the Bushveld Complex with an emphasis on chromitite formation: *Contributions to Mineralogy and Petrology*, v. 175, p. 1–17.
- Vekslar, I.V., Sedunova, A.P., Darin, A.V., Anosova, M.O., Reid, D L., Kaufmann, F.E., Hecht, L., and Trumbull, R.B., 2018, Chemical and

- textural re-equilibration in the UG2 chromitite layer of the Bushveld Complex, South Africa: *Journal of Petrology*, v. 59, p. 1193–1216.
- Ver Hoeve, T.J., Scoates, J.S., Wall, C.J., Weis, D., and Amini, M., 2018, A temperature-composition framework for crystallization of fractionated interstitial melt in the Bushveld Complex from trace element systematics of zircon and rutile: *Journal of Petrology*, v. 59, p. 1383–1416.
- Voigt, M., and von der Handt, A., 2011, Influence of subsolidus processes on the chromium number in spinel in ultramafic rocks: *Contributions to Mineralogy and Petrology*, v. 162, p. 675–689.
- von Gruenewaldt, G., Hatton, C.J., and Merkle, R.K.W., 1986, Platinum-group element-chromitite associations in the Bushveld Complex: *Economic Geology*, v. 81, p. 1067–1079.
- von Gruenewaldt, G., Hulbert, L.J., and Naldrett, A.J., 1989, Contrasting platinum-group element concentration patterns in cumulates of the Bushveld Complex: *Mineralium Deposita*, v. 24, p. 219–229.
- Voordouw, R., Gutzmer, J., and Beukes, N.J., 2009, Intrusive origin for upper group (UG1, UG2) stratiform chromitite seams in the Dwaars River area, Bushveld Complex, South Africa: *Mineralogy and Petrology*, v. 97, p. 75–94.
- Vukmanovic, Z., Barnes, S.J., Reddy, S.M., Godel, B., and Fiorentini, M.L., 2013, Morphology and microstructure of chromite crystals in chromitites from the Merensky reef (Bushveld Complex, South Africa): *Contributions to Mineralogy and Petrology*, v. 165, p. 1031–1050.
- Yudovskaya, M.A., Costin, G., Shilovskikh, V., Chaplygin, I., McCreesh, M., and Kinnaird, J., 2019, Bushveld symplectic and sieve-textured chromite is a result of coupled dissolution-reprecipitation: A comparison with xenocrystic chromite reactions in arc basalt: *Contributions to Mineralogy and Petrology*, v. 174, p. 1–21.



Sarah-Jane Barnes is a professor emerita, Université du Québec Chicoutimi (UQAC). Her main research interests are in ore deposits associated with mafic and ultramafic rocks. Barnes earned her BSc (Hons) from the University of Witwatersrand, her MSc from the University of Cape Town, and her PhD (1983) from the University of Toronto, followed by a postdoctoral fellowship at the Geological Survey of Norway (1984–1986). Her professional employment includes work as a geologist for the Geological Survey of Namibia, as a lecturer at the University of Toronto, and as research associate and professor at UQAC. She was named the Canada Research Chair at UQAC (2004–2017) and holds a number of awards, including Awards Fellow of the Royal Society Canada (2020), Duncan Derry Medal Geological Association of Canada (GAC) (2020), Jean Descarreaux Prize (2016), SEG Distinguished Lecturer (2014), Mineralogical Association Canada Past-Presidents Medal (2007), Gross Medal GAC (1994), and SEG R.A.F. Penrose Gold Medal (2025).